frontiers | Frontiers in Earth Science

ORIGINAL RESEARCH
published: 05 April 2022
doi: 10.3389/feart.2022.836381

Elemental and Isotopic Signatures of Bulk Sedimentary Organic Matter in Shenhu Area, Northern South China Sea

Yuanyuan Li[1,2], Xuemin Xu[3], Lei Pang[2], Ping Guan[2], Yunxin Fang[4], Hailong Lu[2]*, Jianliang Ye[4] and Wenwei Xie[4]*

[1]College of Engineering, Peking University, Beijing, China, [2]Beijing International Center for Gas Hydrate, School of Earth and Space Sciences, Peking University, Beijing, China, [3]National Research Center for Geoanalysis, Beijing, China, [4]MLR Key Laboratory of Marine Mineral Resources, Guangzhou Marine Geological Survey, Ministry of Land and Resources, Guangzhou, China

Hydrate-bearing sediments provide excellent materials for studying the primary sources and diagenetic alterations of organic matter. In this study, the elemental and isotopic signatures of total organic carbon (TOC), total inorganic carbon (TIC), total nitrogen (TN), and total sulfur (TS) are systematically investigated in three hydrate-bearing sediment cores (~240 m) retrieved from the Shenhu area, South China Sea. All sediment layers from three sites are with low TOC content (average 0.35%) with marine and terrestrial mixed sources (-23.6‰ < $\delta^{13}C_{org}$ < -21.4‰). However, the generally low $\delta^{15}N$ (2.49–5.31‰) and C/N ratios (4.35–8.2) and their variation with depth cannot be explained by the terrestrial sources (Pearl River) and marine sources, binary end-member mixing processes. Contribution from lateral allochthonous organic matter from the mountainous river is considered after excluding other possible factors and ingeniously elucidating the organic matter origins. Furthermore, specific layers in W01B and W02B exhibit elevated S/C ratios (up to 2.39), positive bias of $\delta^{34}S$-TS (up to +29.7‰), and negative excursion of $\delta^{13}C$-TIC (up to -8.29‰), which are the characteristics of sustained occurrence of sulfate-driven anaerobic oxidation of methane. The occurrence of coupled carbon–sulfur anomaly may be accompanied by deep hydrocarbon leakage and the formation of hydrate with high saturation.

Keywords: methane seepage, organic matter, gas hydrate, Shenhu area, biogeochemistry, C-N-S

Edited by:
Xiting Liu,
Ocean University of China, China

Reviewed by:
Zhiyong Lin,
University of Hamburg, Germany
Jiarui Liu,
University of California, United States

****Correspondence:***
Yunxin Fang
fangyunxin0825@sina.cn
Hailong Lu
hlu@pku.edu.cn

Specialty section:
This article was submitted to Marine Geoscience, a section of the journal Frontiers in Earth Science

Received: *15 December 2021*
Accepted: *25 February 2022*
Published: *05 April 2022*

Citation:
Li Y, Xu X, Pang L, Guan P, Fang Y, Lu H, Ye J and Xie W (2022) Elemental and Isotopic Signatures of Bulk Sedimentary Organic Matter in Shenhu Area, Northern South China Sea. Front. Earth Sci. 10:836381. doi: 10.3389/feart.2022.836381

1 INTRODUCTION

Natural gas hydrates have been a frontier issue in both industrial and academic research (Kvenvolden, 1995; Collett et al., 2009). Marine geological surveys and drilling expeditions have verified that the Shenhu area, South China Sea (SCS) (**Figures 1A,B**) (Liu et al., 2011a; Trung, 2012; Jiang et al., 2015; He et al., 2016), is one of the most promising exploration targets for gas hydrates and has carried out two test mining in this area in the past 5 years (Wu et al., 2011; Zhang et al., 2014a; Wang et al., 2014; Zhang et al., 2017a; Zhang et al., 2017b; Su et al., 2018).

Gases bounded in hydrate can be divided into microbial gases and thermogenic gases, which are different products during the burial and evolution of sedimentary organic matter (Schoell, 1983). For whatever origin, the provenances and quality (lability) of organic matter in sediments may be the key

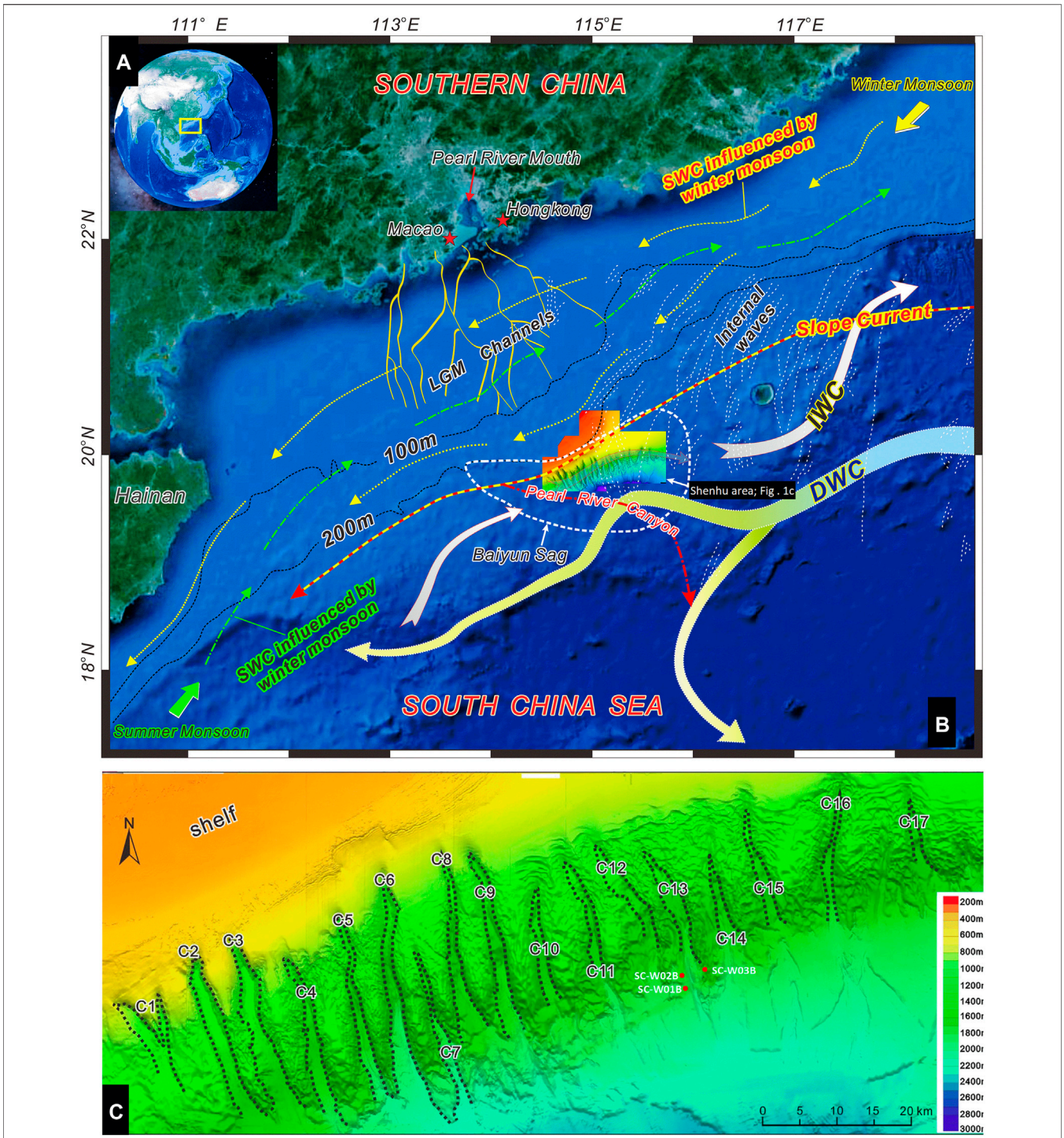

FIGURE 1 | (A) Location of the South China Sea (SCS, from Google Earth). **(B)** Location and regional oceanic circulation model of the Shenhu area, SCS, modified from Wang et al. (2020b). White arrows: intermediate water current; colored arrows: deep-water current; white dashed lines: internal waves (Hsü et al., 2000; Wang et al., 2012; Alford et al., 2015); yellow–red dashed arrow: slope current (Wang et al., 2010). **(C)** Locations of coring sites of GMGS4 (Yang et al., 2017b; Zhang et al., 2019).

factors controlling the accumulation of gas hydrate since it is the source of carbon for a huge number of hydrocarbons bounded in gas hydrate (Kvenvolden, 1995). Terrestrial vascular plants and marine algae have been considered to be optimum precursors for methanogenesis used by microbes in marine settings (Kaneko et al., 2010). A study of organic matter in the hydrate-bearing

sediment of Okinawa trough proposed that terrestrial organic matter is more conducive to the formation of microbial gases (Saito and Suzuki, 2007), verifying that the source and activity of sedimentary organic matter are important factors controlling the formation of hydrate, but the specific mechanism requires further study. Compositional ratios (C/N ratios) and isotopic composition ($\delta^{13}C_{org}$ and $\delta^{15}N$) of organic matter are proxies used to deduce its original properties and transformation processes after deposition, and may provide insights into the gas generation.

The content (TS) and isotopic composition ($\delta^{34}S$) of sulfur can reflect the utilization of different organic precursors and different mineralization pathways by sulfate-reducing bacteria (SRB). In normal methane-free marine sediment where organiclastic sulfate reduction (OSR) is dominated, the generally low availability and high recalcitrance of metabolizable substrates in marine sediments result in low cell-specific sulfate reduction rate, fostering the expression of equilibrium fractionation, leading to large and generally constant sulfur isotope fractionation up to ca. 70‰ (e.g., Sim et al., 2011; Wing and Halevy, 2014; Jørgensen et al., 2019). The amount of formed pyrite is usually limited and eventually depends on the labile organic matter content. However, in certain environments (e.g., methane seeps and probably the sulfate methane transition zone (SMTZ) resides in deeper sediments), the sulfur isotope fractionation can be smaller due to a higher substrate concentration and thus a greater expression of kinetic fractionation. This sulfate-driven anaerobic oxidation of methane (SD-AOM) supplies a large amount of extra HS^- for the formation of pyrite and facilitates the augmentation of authigenic pyrite in the SMTZ (Boetius et al., 2000; Peckmann et al., 2001; Jørgensen et al., 2004; Peketi et al., 2012; Peketi et al., 2015). Therefore, the content and isotopic composition of TS may provide key clues for the SRB-mediated carbon–sulfur biogeochemical cycle (Jørgensen, 2021). Furthermore, fluctuations in sedimentation rates, disproportionation of intermediate sulfur, and other factors may also result in additional isotope fractionation of the TS (Jørgensen et al., 2004; Brunner and Bernasconi, 2005; Peketi et al., 2015; Liu et al., 2019; Liu et al., 2021). In turn, the isotopic composition of TS can provide valuable clues for the complex sulfur cycle.

The content and isotopic signatures of bulk total organic carbon (TOC), total inorganic carbon (TIC), total nitrogen (TN), and total sulfur (TS) were employed in this study to constrain the primary properties of sedimentary organic matter in Shenhu hydrate-bearing sites of the northern South China Sea (NSCS), as well as the response of the sedimentary organic matter under the background of the presence of methane hydrate or potential methane leakage. Our multi-element and multi-isotope studies will deepen our current recognition of the characteristics of organic matter in the hydrate deposit area, as well as the biogeochemical cycle in hydrate systems where methanogenesis and methane oxidation are both ubiquitous.

2 GEOLOGICAL SETTING

Located at the intersection of three tectonic plates, the SCS is the largest passive marginal sea in Western Pacific (**Figure 1A**) (Sun et al., 2006; Xu et al., 2014a). The complex tectonic evolution history and promising resource prospects have made SCS a natural laboratory for marine geology research (Lu et al., 2011; Wang et al., 2020a). The Shenhu drilling area is located in Baiyun Sag, a deep-water depression in the Pearl River Mouth Basin (PRMB) of SCS (Yu, 1990; Pang et al., 2007) (**Figure 1B**). The modern oceanographic background of the SCS was established at 3 Ma, and the flow patterns have been basically unchanged since the Quaternary (Li et al., 2007). The baroclinic gradient below 1500 m in the Luzon Strait leads to the inflow of cold and dense North Pacific Deep Water (NPDW) into the SCS (Qu et al., 2006), bringing the SCS a "sandwich" layered structure characterized by three contour current at different depths: the surface water current (SWC, <350 m), intermediate water current (IWC, 350–1,500 m), and deep-water current (DWC, >1,500 m) (Chen and Wang, 1998; Tian et al., 2006; Zhu et al., 2010; Chen et al., 2014). A continuous westward along-slope current within the depth of SWC is generated subject to the East Asian monsoon and Kuroshio intrusion (Nan et al., 2015). It is noteworthy that the boundaries between these currents are changing spatiotemporally, which can alter the distribution of sediments in the NSCS. In addition, internal waves are often recorded in the mooring systems and remote sensing images in the NSCS (Hsü et al., 2000; Zhao and Alford, 2006; Wang et al., 2012), most of which propagate westward from Luzon (Alford et al., 2015; Ma et al., 2016; Tang et al., 2018). The mooring system shows that, in the eastern part of Baiyun Sag, the internal solitary waves indirectly impact the north slope and consequently generate strong bottom current along the slope, with a maximum velocity more than 40 cm/s (Lin et al., 2014). Besides the internal waves, internal tides have also been recorded in the mooring system, which contributes to the re-suspension and transport of the sediment on the shelf and slope of the NSCS (Reeder et al., 2011; Ma et al., 2016; Geng et al., 2017).

3 MATERIALS AND METHODS

The samples are retrieved from expedition GMGS4 which was carried out on the geotechnical drilling vessel Fugro Voyager in 2016 (Yang et al., 2017b). The water depth of the three sites is ~1,285 m, 1,274 m, and 1,310 m, respectively (**Figure 1C**).

The content of TOC along with TS was determined by Leco CS744 Carbon/Sulfur Determinator after removing the carbonate with 2 mol/L HCl. The measurement precision is 0.5% RSD for carbon and 1.5% RSD for sulfur. The isotope of organic carbon ($\delta^{13}C_{org}$) and bulk nitrogen ($\delta^{15}N$) was determined by Elementar Isoprime 100 with analytical reproducibility better than 0.1‰ for $\delta^{13}C_{org}$ and 0.15% for $\delta^{15}N$. The nitrogen content (TN) was analyzed by a vario PYRO cube analyzer with external precision better than 0.1%. The above element and isotope analyses were conducted at the National Research Center for Geoanalysis, China Geological Survey (CGS).

The $\delta^{13}C$ detection of the TIC ($\delta^{13}C$-TIC) phase was performed on an isotope ratio mass spectrometer (IRMS, Thermo Fisher Delta V Advantage) coupled with an automated carbonate preparation device (Gas Bench II) at Peking University. The analytical precision of $\delta^{13}C$ is smaller than 0.2‰.

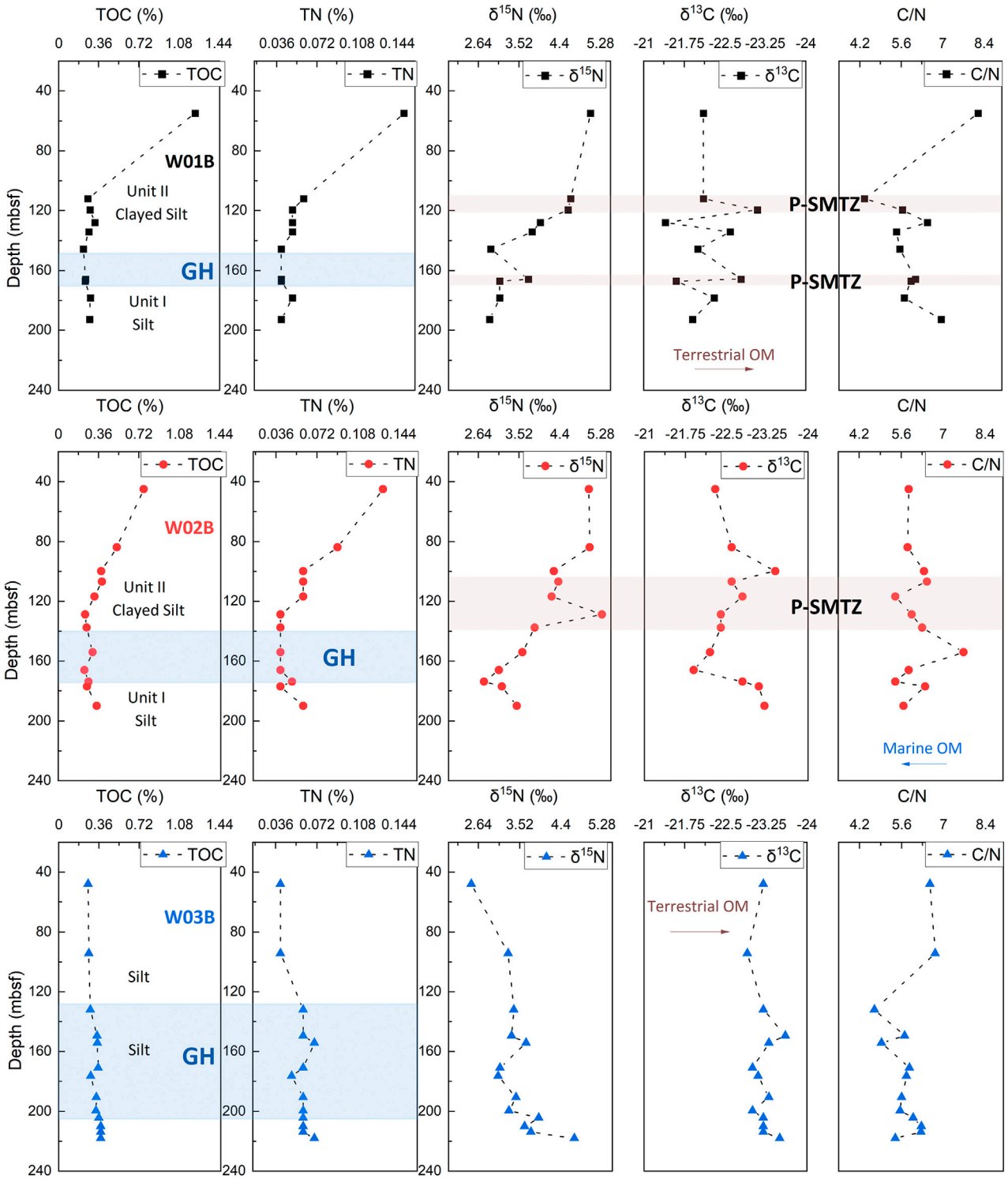

FIGURE 2 | Depth profiles of TOC, TN, $\delta^{15}N$, $\delta^{13}C_{org}$, and C/N ratio for W01B, W02B, and W03B from the Shenhu area, SCS. The blue shaded areas indicate the hydrate-bearing layer, and the pink shaded areas imply the possible paleo-sulfate methane transition zone (SMTZ).

The sulfur isotope of TS (^{34}S-TS) was analyzed at the Oxy-Anion Stable Isotope Consortium (OASIC) at Louisiana State University. Bulk-powdered samples of 10–15 mg were weighted, and 2 mg V_2O_5 was added to a tin cup for analyses on a gas-source isotope ratio mass spectrometer (GS-IRMS, Isoprime 100) coupled with an elemental analyzer (EA). The standard deviation associated with

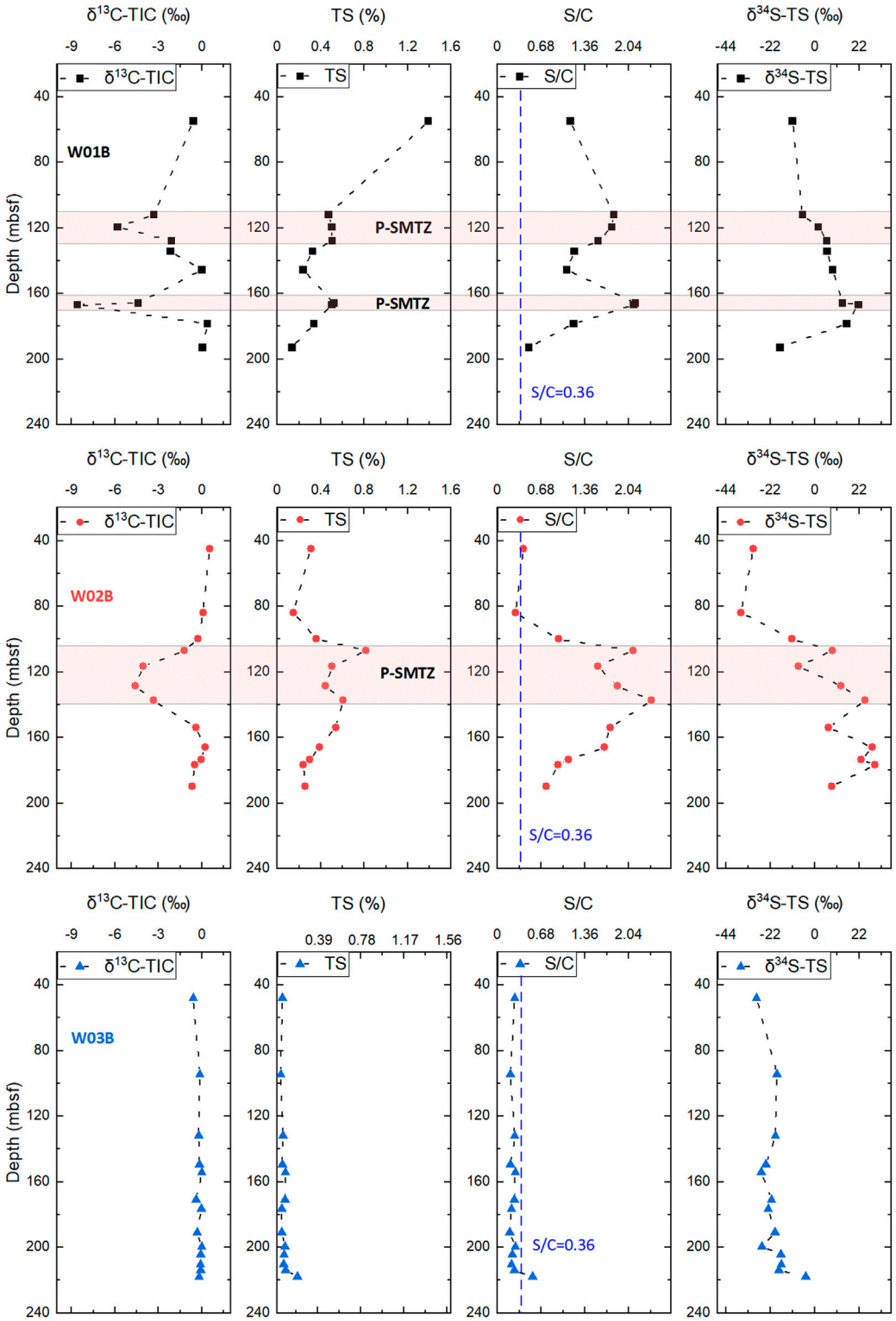

FIGURE 3 | Depth profiles of δ^{13}C-TIC, TS, S/C ratio, and δ^{34}S-TS for W01B, W02B, and W03B from the Shenhu area, SCS. The pink shaded areas imply the possible P-SMTZ.

$\delta^{34}S$ analysis is less than 0.3‰. The $\delta^{15}N$, $\delta^{13}C$, and ^{34}S values are expressed as the delta (δ) notation relative to the atmospheric N_2, Vienna Pee Dee Belemnite (VPDB), and Vienna Canyon Diablo Troilite (VCDT), respectively.

4 RESULTS

TOC contents of sediments from sites W01B and W02B decrease exponentially with depth from 1.17 to 0.18%, while that of W03B slightly increases with depth from 0.04 to 0.26% (**Supplementary Table S1**) (**Figure 2**). The TN contents of sediments from the three sites have similar trends to the TOC contents which vary from 0.03 to 0.16% (**Supplementary Table S1**) (**Figure 2**). The depth variation of $\delta^{15}N$ of bulk sediments from three sites is basically similar to that of the TOC and TN, ranging from 2.48 to 5.06‰ (**Supplementary Table S1**) (**Figure 2**). The $\delta^{13}C_{org}$ of sediments from three sites confines to -23.1–21.4‰, -23.4–21.9‰, and -23.6–22.9‰, respectively, among which W01B and W02B sites have higher isotope composition than W03B (**Supplementary Table S1**) (**Figure 2**). C/N ratios for sediments from W01B and W02B have high values at specific layers (170 mbsf for W01B and 130 mbsf for W02B), which are in the range of 4.23–14.81 and 3.89–10.65, respectively (**Supplementary Table S1**) (**Figure 2**), whereas that of W03B shows steadiness with a depth around an average value of 1.9%. The $\delta^{13}C$-TIC values of the sediment are mostly around 0‰, with obvious negative bias in certain intervals (120 mbsf and 170 mbsf for W01B; around 116–137mbsf for W02B) (**Supplementary Table S1**) (**Figure 2**).

The TS content of sediments from W01B tends to decrease with depth, with relatively slight increases at 120mbsf (0.51%) and 167mbsf (0.52%) (**Supplementary Table S1**) (**Figure 3**). The TS content of sediments from W02B has low values (0.15–0.39%) at the top and bottom layers but increases in the middle interval (0.44–0.82%), especially at 106.86mbsf (0.81%) (**Supplementary Table S1**) (**Figure 3**). However, the TS content of sediments from W03B is lower overall (with an average value of 0.08%) and varies little with depth, except for a slightly high value of 0.21% at the deepest layer (**Supplementary Table S1**) (**Figure 3**). The S/C ratios of sediments from W01B and W02B are basically greater than 0.36, with lower values in the shallower and deeper layers (**Supplementary Table S1**) (**Figure 3**). There are different increases in the intermediate layer, and the highest value can reach 2.39%. Like the depth variation of TS, the S/C ratios of sediments from W03B also have minor variation through the depth record, with an average value of 0.26% (**Supplementary Table S1**) (**Figure 3**). The $\delta^{34}S$-TS of sediments from W01B and W02B tends to increase with depth, except for the unique low value in the deepest layer of W01B, while $\delta^{34}S$-TS of sediments from W03B remains relatively stable with depth, with an average value of -21.48‰ (**Supplementary Table S1**) (**Figure 3**).

5 DISCUSSIONS

5.1 Provenances of the Organic Matter

The C/N ratios and $\delta^{13}C_{org}$ of deposited organic matter are generally adopted to recognize its provenances since marine and terrestrial organic matter is with distinct C/N ratios and $\delta^{13}C_{org}$ values (Sackett and Thompson, 1963; Hedges and Mann, 1979; Calvert and Fontugne, 1987; Jasper and Gagosian, 1989). Typical marine organic matter is with C/N ratios in the range of 4–10 and $\delta^{13}C_{org}$ values between -19 and -22‰ (Premuzic et al., 1982; Fontugne and Jouanneau, 1987; Emerson and Hedges, 1988; O'Leary, 1988; Jasper and Gagosian, 1989; Goni and Hedges, 1995; Aksu et al., 1999). In contrast, typical terrestrial organic matter is usually with C/N ratios greater than 20 and $\delta^{13}C_{org}$ values between -26 and -28‰ (Emerson and Hedges, 1988; Meyers, 1994; Prahl et al., 1994). The Shenhu area is located in the PRMB in the NSCS, which is generally considered to mainly receive mixing organic matter from marine autochthonous and terrestrial allochthonous sources of the Pearl River estuary (PRE). It has been reported that $\delta^{13}C_{org}$ values of terrestrial organic material deposited in the PRE and marine organic matter are -25.5‰ and -22.1‰, respectively, and C/N ratio values are 14–20 and 6.6, respectively (Hu et al., 2006; Liu et al., 2007a; Gaye et al., 2009; Kao et al., 2012; Zhang et al., 2014b).

In general, the increase of C/N ratios and the negative bias of $\delta^{13}C_{org}$ indicate the increased contribution of terrestrial organic matter. However, in this study, C/N ratios and $\delta^{13}C_{org}$ do not show uniform changes, that is, $\delta^{13}C_{org}$ does not show negative excursion in the C/N ratio increased horizon (**Figure 2**). Specifically, for example, the $\delta^{13}C_{org}$ of sediment from station W03B is the lowest (i.e., most terrestrial contribution) among the three sites, but its C/N ratios are almost the smallest among the three sites (**Figure 2**), which means when the $\delta^{13}C_{org}$ record points to an increase of terrestrial inputs, the C/N ratio tendency does not support it. Indications from different organic geochemical indexes of the bulk sediment are contradictory.

Furthermore, it has been reported that the $\delta^{15}N$ of the terrestrial surface sediments in the PRE ranges from 6.2 to 7.1‰, which is 1–2‰ higher than that of the modern nitracline (Wong et al., 2002; Gaye et al., 2009). Besides, except for $\delta^{15}N$ recorded at ODP 1144 in the NSCS which has been suggested to be related to the sediment drifts and allochthonous sources of nitrogen (Higginson et al., 2003; Kienast et al., 2005), most of the published $\delta^{15}N$ values in the SCS do not show the significant glacial–interglacial difference (Kienast, 2000), especially compared to the $\delta^{15}N$ of foraminifera-bound nitrogen (Wang et al., 2018), indicating that the $\delta^{15}N$ of marine nitrate was relatively constant (Kienast, 2000). The $\delta^{15}N$ of the marine source organic matter of SCS has been recorded to be around 6.2‰ (Liu et al., 2007a; Kao et al., 2012). However, the $\delta^{15}N$ of sedimentary organic matter from this study ranged from 2.48 to 5.31‰, with an average value of 3.74‰ (**Supplementary Table S1**) (**Figure 2**). The lower $\delta^{15}N$ values indicate that the provenance of the organic matter cannot only be from the PRE and the marine autochthonous productivity, there must also be a lower $\delta^{15}N$ end-member contributing to the bulk organic matter, or some post-deposition processes have altered the original isotope signature of organic matter.

In addition, the differences in the isotopic composition and content of the bulk organic matter between the three sites have also remained unclear, which means further insights need to be

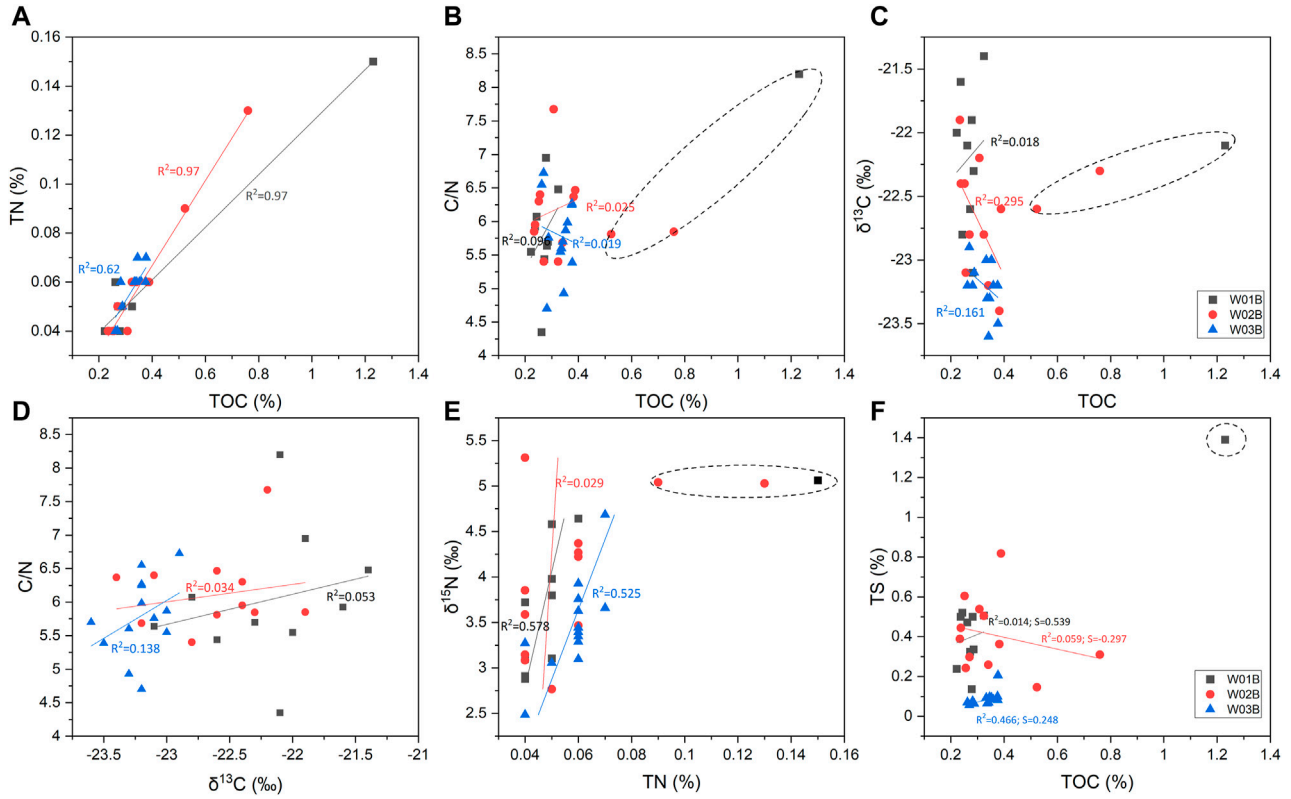

FIGURE 4 | Scatterplots of **(A)** TN versus TOC, **(B)** C/N ratio versus TOC, **(C)** $\delta^{13}C_{org}$ versus TOC, **(D)** C/N ratio versus $\delta^{13}C_{org}$, **(E)** $\delta^{15}N$ versus TN, and **(F)** TS versus TOC of the sediment of W01B, W02B, and W03B from the Shenhu area, SCS.

explored into the interpretation of the provenance and distribution of the bulk organic matter of the three sites (**Figure 2**). Given the very close proximity (on either side of the ridge of a deep-water canyon, horizontal distance less than 10 km, water depth difference less than 30 m) of the three core sites, any sedimentary factors conceived to interpret the prominent differences among these three sites would have to be able to accommodate such large differences on such small spatial patterns. Because the three sites are located under the identical nutrient regime and biogeographic zone, the discrepancies between them are implausible to reflect the true gradient of the marine surface biochemistry or the original $\delta^{15}N$ signal. Here, we take inorganic nitrogen, diagenetic alteration, methane-associated activities, and lateral allochthonous sediments into consideration.

5.1.1 Inorganic Nitrogen

The inorganic nitrogen comes directly from terrestrial input or ammonia derived from the degradation of organic matter during diagenesis (Meyers, 1997; Hu et al., 2006). In the former case, terrestrial inorganic nitrogen is usually more depleted in ^{15}N compared to marine organic nitrogen (e.g., Schubert and Calvert (2001); Kienast et al. (2005)), so the mixing of the inorganic nitrogen can decrease the $\delta^{15}N$ signal. In contrast, for the latter case, the adsorption of ammonium nitrogen on clay minerals can reduce the C/N ratios inherited from the primary source characteristics (Müller, 1977; Arnaboldi and Meyers, 2006).

The proportion of inorganic nitrogen to bulk sediments can be calculated by the value at the y-intercept of the TN versus TOC cross-plots (Nijenhuis and De Lange, 2000; Calvert, 2004; Arnaboldi and Meyers, 2006). The TOC versus TN of the three sites exhibits good linearity indicating that the bulk organic matter phase in the sediment is relatively uniform. There is no/minor intercept on the TN axis (**Figure 4A**), which suggests that the content of clay-bound nitrogen in these three sites is negligible. Moreover, Kienast et al. (2005) analyzed the isotope composition of inorganic nitrogen from the SCS and reported that inorganic nitrogen in the SCS has $\delta^{15}N$ values within the scope of 3.1–4.8‰. However, the lightest nitrogen isotope in this study is 2.46‰, which means that the inorganic nitrogen should not be the dominant ^{15}N-depleted end-member for the mixing model.

5.1.2 Diagenetic Alteration

As for the C/N ratio, there is no correlation between the C/N ratio and TOC (**Figure 4B**), and the C/N ratio has no systematic variation with depth (**Figure 2**), suggesting the diagenetic alteration is an insignificant or not dominated factor for the C/N ratio discrepancies of the organic matter. It has been reported that the ^{13}C-enriched organic proteins and carbohydrates will be preferentially decomposed during

diagenesis, thus changing the primary $\delta^{13}C$ composition of the organic matter, but the fractionation is relatively insignificant (<-2‰ (McArthur et al., 1992)). In this study, the overall $\delta^{13}C_{org}$ appears to be independent of TOC content and C/N ratio (**Figures 4C,D**), indicating diagenesis has not appreciably affected $\delta^{13}C_{org}$ values (Fontugne and Duplessy, 1986; Calvert and Fontugne, 1987; Calvert et al., 1992). The ammonium nitrogen released during diagenesis is ^{15}N-depleted, and the $\delta^{15}N$ of residual sedimentary nitrogen will be increased by ~2.5‰, associated with the type and intensity of microbial activity (Freudenthal et al., 2001; Lehmann et al., 2002), which simultaneously dampen the C/N ratio. In respect of $\delta^{15}N$, among the three sites, only the $\delta^{15}N$ of W03B increases with depth, but contrary to the decrease of nitrogen content that diagenesis should have caused, the TN of W03B increased with depth (**Figure 4E**), which argues against the law of diagenetic modification.

5.1.3 Impact From Hydrate Dissociation or Methane Seepage

Only a few studies have described the organic geochemical characteristics of hydrate-bearing sediments. Yu et al. (2006) found that the presence of natural gas hydrate changed the diagenetic evolution trajectory of organic carbon and nitrogen elements in hydrate-bearing sediments of Hydrate Ridge and found that the $\delta^{15}N$ value (~2%) and C/N ratio of sediments at the hydrate-bearing layer declined simultaneously, but the $\delta^{13}C$ value was relatively high. In that case, the increase of nitrogen content and the loss of ^{15}N in the hydrate stability zone were interpreted to be related to the nitrogen fixation of bacteria and archaea in the sediments where gas hydrate is developed (Yu et al., 2006). Recent studies have found negative excursions of $\delta^{15}N$ in the SMTZ of the sediment from Haima seeps of the SCS, and it is pointed out that the anaerobic methanotrophic (ANME) archaea can intermediate nitrogen fixation and ammonium assimilation (Hu et al., 2020). ^{14}N is considered to be preferentially utilized during these processes and thereby cause the negative excursion of $\delta^{15}N$ (Hu et al., 2020).

In this study, the $\delta^{15}N$ depth records of W01B and W02B seem to be relatively lower in the deeper part which bears gas hydrate and conforms to the inference of Yu et al. (2006) (**Figure 2**), while concerning W03B, it presents an opposite trend and has a higher $\delta^{15}N$ in the hydrate-bearing zone. Therefore, the existence of hydrate does not seem to be the main cause of the nitrogen isotope variation. We also identified several SMTZs in W01B and W02B by the elevated S/C ratio and excursion of $\delta^{13}C$-TIC and $\delta^{34}S$-TS (see details in the 5.3 chapter), which assist us to find the potential effect of ANME archaea or AOM consortia. But it seems that there is no negative $\delta^{15}N$ excursion in the identified SMTZ. Moreover, the SMTZ has not been recognized at W03B, but it has the most negative $\delta^{15}N$ among the three sites, so the effect of AOM seems limited to cause the variation of $\delta^{15}N$ depth record.

Apart from nitrogen fixation and ammonium assimilation, denitrification (especially coupled with AOM) and anaerobic ammonium oxidation are widespread in the shallow subsurface of the continental margin. However, their impact on nitrogen stable isotope compositions of bulk sediments is negligible (Lehmann et al., 2007). Furthermore, amorphous carbon has been identified and isolated from ANME archaea and select methanogens in the previous study, which was characterized by strong ^{13}C depletion ($\delta^{13}C$–60‰) and high C/N ratios (17.5–58.4) (Allen et al., 2021). Therefore, the formation of amorphous carbon in natural sediments will significantly lower its $\delta^{13}C_{org}$ value and elevate its C/N ratios. The proxies of sediments from the identified SMTZ do not exhibit such synchronous variation trends, indicating that the role of amorphous carbon is negligible in this study.

5.1.4 Lateral Allochthonous Input

According to the data of the sediment trap, the collected particle N flux below 2000 m in the SCS is higher than that in the upper euphotic zone; these additional particulate N fluxes are thought to be due to lateral transport, which carried ^{15}N-depleted particles that originated from the Kaoping Canyon (Yang et al., 2017a). The Kaoping River in the southwest of Taiwan island was reported to import 36–40 Mt/yr particulate matter into the SCS, of which around 85% was transported to the deep-sea basin of the SCS through the Kaoping Canyon (Huh et al., 2009). The lateral particulate organic matter (POM) inputs to the basin tend to have a lighter nitrogen isotopic signature (Kao et al., 2006; Gaye et al., 2009; Yang et al., 2017a).

After eliminating the possible interference from the above factors, we consider this lateral allochthonous input and comprehensively adopt the $\delta^{15}N$, $\delta^{13}C_{org}$, and C/N (or N/C) ratio proxies to constrain the potential sources of the organic matter (**Figure 5**). Potential source end-members of organic matter in the NSCS include the marine autochthonous source, the PRE, and mountainous rivers from Taiwan and Luzon. The published values of the above end-members are compiled in **Figure 5** (Hu et al., 2006; Kao et al., 2006; Liu et al., 2007a; Gaye et al., 2009; Kao et al., 2012; Zhang et al., 2014b; Yang et al., 2017a). Overall, according to the relationship between $\delta^{13}C$ values, N/C ratios, and $\delta^{15}N$ values, the organic matter of sediments from this study basically falls into the mixing zone of mountainous river sources and marine sources (**Figure 5**), indicating the mixed characteristic of these end-members, which is consistent with the conclusion of the sources of detrital clastic components of the studied samples (unpublished data). In brief, from content ratios and isotope composition cross-plots, we hypothesize that the mountainous rivers are a potential source of organic matter transported laterally to the study area by possible contour current, which will be discussed in detail in the next chapter (Liu et al., 2010b; Schroeder et al., 2015; Liu et al., 2016).

The introduction of the Taiwan mountainous river provenance end-member provides clues for the unresolved question we raised earlier. First, the variations of C/N ratios and $\delta^{13}C_{org}$ of sediment is asynchronously in the depth profile, may ascribe to the lower C/N ratios of Taiwan mountainous riverine organic matter which different from the conventional terrestrial organic matter (high C/N ratios). In this case, the addition of terrestrial organic matter could not significantly elevate the C/N ratio and solely lower the $\delta^{13}C_{org}$ of sediment. Second, the Taiwan mountainous river end-member

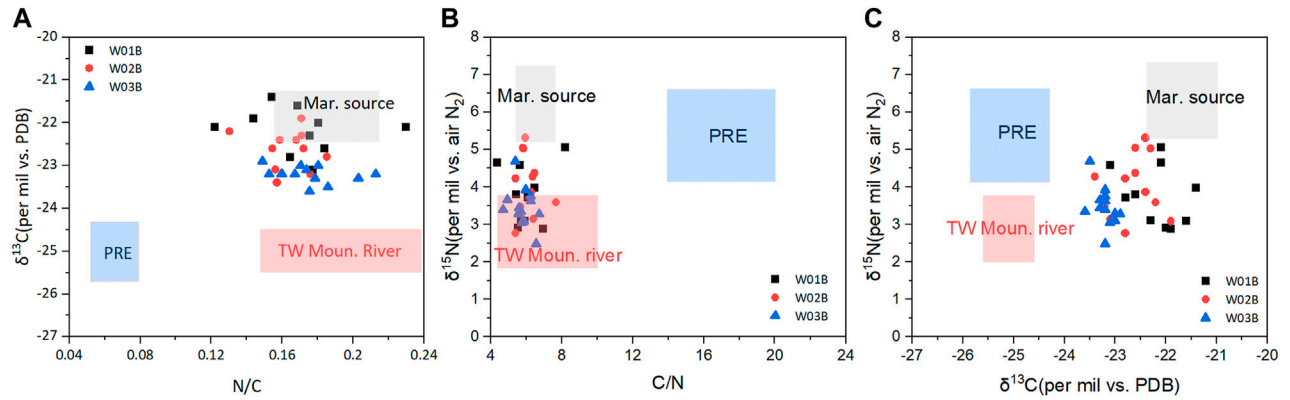

FIGURE 5 | Cross-plots of **(A)** N/C ratio versus $\delta^{13}C$, **(B)** $\delta^{15}N$ versus C/N ratio, and **(C)** $\delta^{15}N$ versus $\delta^{13}C$, modified from Yang J.-Y. T. et al. (2017). The gray shaded areas indicate marine source (Mar. source) organic matter (Liu K.-K. et al., 2007; Kao et al., 2012). The blue shaded areas represent the organic matter from the Pearl River estuary (PRE) (Hu et al., 2006; Liu K.-K. et al., 2007; Gaye et al., 2009; Zhang et al., 2014b). The pink shaded areas symbolize organic matter from the Taiwan mountainous river (TW Moun. river) (Kao et al., 2006; Gaye et al., 2009; Yang J.-Y. T. et al., 2017).

provides a ^{15}N depleted end-member, which can help to explain that the $\delta^{15}N$ of our samples can be as low as 2.46‰ under the circumstance that the PRE and marine organic matter both have a high $\delta^{15}N$ signature (4.2–6.6‰ and 6.2 ± 1‰, respectively). Third, the provenance of Taiwan indicates the complex hydrodynamic flow field in the Shenhu area, especially the influence of contour current. Combined with the existing geophysical studies, we believe that the samples in this study are products of complex redeposition, and the distribution of geochemical characteristics of sediments is closely related to hydrodynamic conditions (Su et al., 2019; Su et al., 2020; Su et al., 2021).

5.2 Implication From the Provenance

Given the proximity of the Pearl River and the NSCS, especially during the period of low sea level, it has been generally accepted that the Pearl River has supplied a large amount of terrigenous detritus to the NSCS, while studies in recent years suggest that the detrital materials derived from the Pearl River are mostly transported by coastal currents to the southwest, and most of them are deposited in the inner and/or middle shelf (e.g., Liu J. et al. (2011); Ge et al. (2014)). Erosional weathered sediments from Taiwan may be the main source of detrital materials in the slope of NSCS (Wan et al., 2010; Liu et al., 2013; Liu et al., 2014; Huang et al., 2016). The Pearl River is the third largest river in China, which transports about 80 × 10^6 ton/yr of sediments into the western part of the SCS (Milliman and Farnsworth, 2011). Although the rivers originated from southwestern Taiwan have relatively small drainage areas compared to the Pearl River, their annual sediment load can reach 70 × 10^6 ton/yr, which falls within a considerable range with the Pearl River (Milliman and Meade, 1983; Wang, 2003). Thus, terrestrial sediments derived from Taiwan play an important role in the deposition of the NSCS. A recent study about sediment traps suggests that sediments of Taiwan origin can be transported to the Xisha Trough over 1,000 km (Liu et al., 2014).

The modern current circulation system of the SCS provides favorable transportation conditions for the import of sediments from Taiwan in the study area. The westward Guangdong coastal current and coastal current can bring a large amount of Taiwan-sourced sediments into the study area during the period of prevailing northeast monsoon caused by the high atmospheric pressure over Central Asia (Fang et al., 2012). Moreover, driven by the perennial SCS branch of the Kuroshio (SCSBK) and SCS warm current, Taiwan-derived sediments are transported southwest to the Dongsha Islands and Shenhu area (Liu et al., 2010a; Liu et al., 2010b). Previous studies have also proposed that sediments from Taiwan were delivered to the slopes of the Dongsha Islands through the Luzon Strait by deep-water bottom currents (Shao et al., 2001; Lüdmann, 2005; Liu et al., 2010b; Wan et al., 2010). A recent study emphasized the importance of surface-generated mesoscale eddies for the transport of island-derived sediments from Taiwan to the NSCS (Zhang et al., 2014c).

To further confirm our conclusions, studies concerning the sources of detrital materials around the Shenhu area were summarized, which mainly used clay minerals and major and trace element composition. Different tectonic settings, source rock types, and climate conditions can conjunctively generate distinctive weathering intensities and therefore diverse weathering products. Ascribed to the stable craton along with warm and humid climate conditions, the widely exposed granites in South China undergo strong chemical weathering (high chemical index of alteration (CIA), **Figure 6A**) and produce clay end-members dominated by kaolinite (**Figure 6B**) (Liu et al., 2007b). Under the background of rapid uplift since the Pliocene, the exposed tertiary rocks in Taiwan experienced intense and rapid physical weathering (low CIA, **Figure 6A**), resulting in the clay end-member dominated by illite and chlorite (**Figure 6B**) (Liu et al., 2008; Liu et al., 2010b). Moreover, the Cenozoic eruptive basaltic andesites in the Luzon Arc formed a large amount of smectite through chemical weathering (**Figure 6B**)

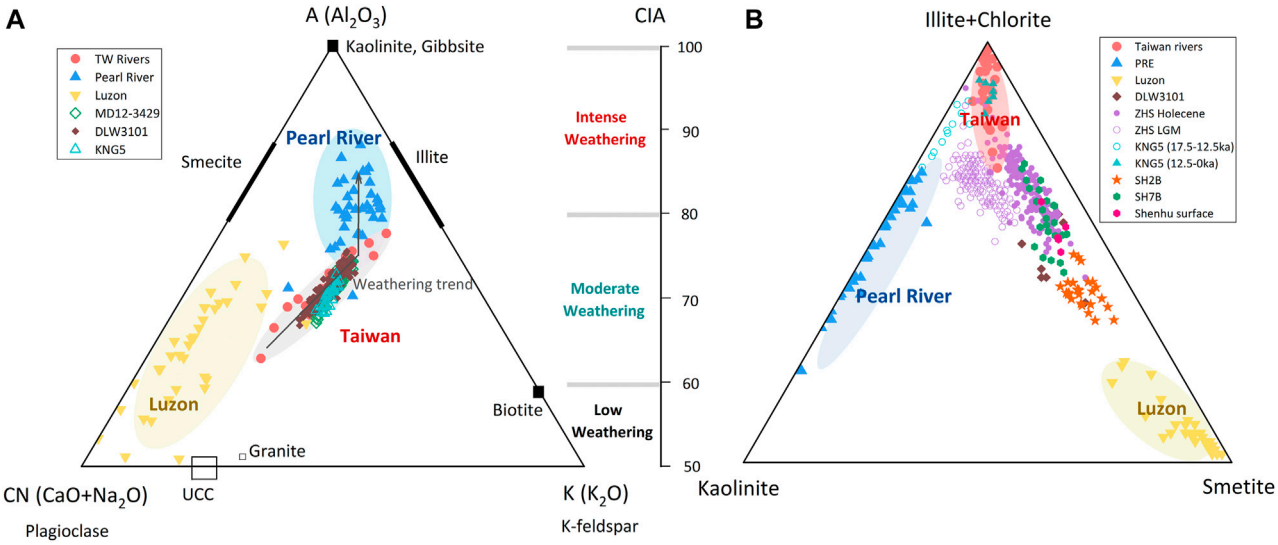

FIGURE 6 | Compilation of major element composition **(A)** and clay mineral proportion **(B)** of sediments from the Shenhu area, SCS. Data of the Shenhu surface sediment from Xu W. et al. (2014); SH2B and SH7B from Lu et al. (2009); DLW3101 from Hu et al. (2021); ZHS 176 from Ge et al. (2010) and Hu et al. (2021); KNG5 from Huang et al. (2011), Huang et al. (2016), and Liu et al. (2017); and MD12-3429 from Hu et al. (2021).

(Liu et al., 2009). The distinct weathering intensity and clay mineral composition assist us to identify the sources of sediments in the SCS. For the Shenhu area, published clay mineral composition of the upper slope (DLW3101), middle slope (surface sediment), and lower slope (SH7B, SH2B) all indicates a comparable contribution from Taiwan and the Luzon Island which have a comparable content of smectite and illite + chlorite (**Figure 6B**). Nevertheless, the ZHS 176 site (eastern part of Shenhu) and KNG5 (western part of Shenhu) are also from around the Shenhu area but show a temporal change, with contribution from Taiwan–Luzon being relatively higher during the Holocene high sea-level period, while the contribution from South China (Pearl River) increases during the low sea-level period, especially in the Last Glacial Maximum (**Figure 6B**). Moreover, the latest data on rare earth elements (REEs) also show that the provenance of Shenhu area has been contributed by the Taiwan end-member (Xiao et al., 2021).

All the above data indicate that the sedimentary pattern of Shenhu area is quite complex, but one thing we can be sure of is that the contribution from the Taiwan-Luzon end-member cannot be ignored in the deposition of Shenhu area. The clay mineral and REE composition of the upper canyon (DLW3101) or inter-canyon (SH2B, SH7B, and surface sediment) all declare that it is entirely possible that the sediments of Shenhu area partially originated from the Taiwan Island.

5.3 Indications of Methane Seepage

Pyrite in sediments is generally formed by SRB via OSR in normal marine sedimentary environments (**Eq. 1**, (Jørgensen (1982)). Reactive iron, labile organic matter, and dissolved sulfate are the main factors controlling the content of authigenic pyrite during this process (Berner, 1982; Jørgensen, 1982; Berner, 1984):

$$CH_2O + SO_4^{2-} \rightarrow 2HCO_3^- + H_2S \quad (1)$$

Under these conditions, there will be a prominent positive correlation between TS and TOC in the sediments, and the S/C ratios are relatively constant around 0.1–0.5, with an average of 0.36 (Berner, 1982; Berner, 1984). The amount of formed pyrite is usually limited in this case because the formation rate is relatively low and the amount eventually formed usually depends on the labile organic matter content. During the OSR, ^{32}S is preferentially utilized than ^{34}S, resulting in ^{34}S-depleted sulfides and ^{34}S-enriched residual sulfates. As mentioned before, the $\delta^{34}S$ value of sulfide can be 66‰ lower than that of seawater sulfate (+20.3‰) at the initial stages of OSR, which is calculated to be around -45‰ (Sim et al., 2011; Borowski et al., 2013; Wing and Halevy, 2014).

In contrast, in hydrate-bearing sediments, the dissociation of gas hydrate will release large quantities of methane and enhance the SD-AOM (**Eqs 2**, **3**), which generates additional HS^- for the formation of pyrite and results in the enrichment of the pyrite in the SMTZ (Boetius et al., 2000; Peckmann et al., 2001; Jørgensen et al., 2004; Peketi et al., 2012; 2015). Simultaneously, this process will increase the TS content and the S/C ratio of the sediment and make TS and TOC lose their linear relationship in OSR (Boetius et al., 2000; Hill et al., 2004; Hill et al., 2011; Joseph et al., 2013):

$$CH_4 + SO_4^{2-} \rightarrow HCO_3^- + HS^- + H_2O \quad (2)$$

$$HS^- + Fe^{2+} \rightarrow FeS \rightarrow FeS_2 \quad (3)$$

The SD-AOM occurring within the SMTZ consumes down-diffused sulfate, which preferentially metabolizes ^{32}S, thereby

enriching ^{34}S in the residual sulfate (Jørgensen et al., 2004; Deusner et al., 2014; Antler et al., 2015). In general, the ^{34}S-enriched sulfide presented in the later SD-AOM dominated stage after ^{34}S-depleted pyrite derived from OSR has formed (Lin et al., 2016; Shawar et al., 2018; Liu et al., 2020). In hydrate-bearing environments, the occurrence of ^{34}S-enriched pyrite in the formation usually can be used as an indicator of significant SD-AOM fueled by continuous methane release to the SMTZ and to discern the paleo-SMTZ (e.g., Peketi et al. (2012); Borowski et al. (2013); Peketi et al. (2015)).

Besides, HCO_3^- produced from AOM subsequently reacted with surrounding Ca^{2+} and Mg^{2+}, forming authigenic carbonate minerals such as aragonite and high-Mg calcite and dolomite (**Eq. 2**) (Greinert et al., 2001; Feng et al., 2018). As a geological archive of cold seepage events, seepage authigenic carbonate minerals are generally characterized by extremely depleted ^{13}C composition inherited from methane (e.g., Rodriguez et al. (2000); Peckmann and Thiel (2004); Ussler and Paull (2008); Lu et al. (2018)):

$$Ca^{2+} + 2HCO_3^- \rightarrow CaCO_3 + CO_2 + H_2O \quad (4)$$

Therefore, the abnormally high pyrite content, elevated S/C ratios, ^{34}S-enriched pyrite, and ^{13}C-depleted TIC can be adopted as proxies for discerning the position of current and paleo-SMTZ in the sediment.

From the cross-plot of TS and TOC, we can see that the TS of W03B has a good correlation with the TOC ($R^2 = 0.466$) and the slope of the fitting line (S = 0.248) approximates the typical OSR value (**Figure 4F**). Besides, the S/C ratio (ca. 0.26), $\delta^{34}S$-TS (ca. -21.48‰), and near-zero of $\delta^{13}C$-TIC (**Figure 3**) without significant variation jointly imply that W03B has no signal of methane seepage or the seepage is too weak to leave geochemical indicators, and the sulfate reduction at W03B may be mainly dominated by OSR. However, the $\delta^{34}S$-TS (ca. -21.48‰) of this OSR-dominated site exhibits a higher value than the lower range of pyrite due to OSR (-45‰, assuming isotope fractionation up to 66‰), which may be ascribed to the mixing of ^{34}S-depleted pyrite and ^{34}S-enriched organic-bound sulfur. The organic sulfur in marine sediments is enriched for ^{34}S more than pyrite, and its $\delta^{34}S$ value is 5–15‰ higher than that of pyrite, with an average value of 10‰ (Anderson and Pratt, 1995).

However, the TOC and TS of W01B and W02B have no good correlation (**Figure 4F**) ($R^2 = 0.014$; $R^2 = 0.059$), indicating that, for W01B and W02B, methane may have been involved in the sulfate reduction. In addition, there are negative excursions of $\delta^{13}C$-TIC near 120 mbsf and 167 mbsf for W01B and 120 mbsf for W02B (**Figure 3**), suggesting the presence of authigenic methane-origin carbonate in these layers. Besides, the elevated S/C ratio and $\delta^{34}S$-TS (**Figure 3**) are also consistent with this inference, indicating the additional ^{34}S-enriched pyrite generated by the SD-AOM, further specifying the presence of paleo-SMTZ. These phenomena associated with methane seepage or hydrocarbon leakage are consistent with the discrepancies of gas origin and hydrate saturation among the three sites. It has been reported that the gas hydrate from W03B is dominated by microbial gas ($\delta^{13}C\text{-}CH_4$ ~ -65‰) with relatively low hydrate saturation (<40%), while gases from W01B and W02B are with considerable contribution from deep thermogenic hydrocarbons ($\delta^{13}C\text{-}CH_4$ ~ -47‰) with high saturation (up to 60%) (Yang et al., 2017b; Zhang et al., 2019). The coupled carbon–sulfur anomalies may be ascribed to the deep hydrocarbon leakage, which provides sufficient gases for hydrate formation and leaves geochemical indicators in the surrounding sediments. More hydrate-bearing sediments with different gas origins are required for further investigation.

6 CONCLUSION

Multi-element and multi-isotope approaches are adopted to study the sources of organic matter and biogeochemical cycle in hydrate-bearing sediments from three long sedimentary sites in the Shenhu area. The vertical variation and lateral distribution of organic matter in sediments with generally low $\delta^{15}N$ and C/N ratios cannot be explained by the two end-member (terrestrial input from the Pearl River and marine input) mixing processes. Contribution from lateral allochthonous organic matter from the mountainous river is considered after excluding the possible effect of inorganic nitrogen, diagenetic alteration, and methane metabolic activities. The introduction of this end-member ingeniously explains the results of this study and is supported by the previous provenance analyses of detrital clastic fraction in the Shenhu area. Moreover, the coupled carbon–sulfur data (elevated S/C ratio, enriched ^{34}S of TS, and negative excursion of $\delta^{13}C$-TIC) reveal sustained occurrence of SD-AOM at sites W01B and W02B but not at W03B. The discrepancies of C–S responses might be related to the different origins of hydrate-bounded gas and the distribution of hydrate concentration among the three sites.

DATA AVAILABILITY STATEMENT

The original contributions presented in the study are included in the article/**Supplementary Material**, further inquiries can be directed to the corresponding authors.

AUTHOR CONTRIBUTIONS

HL and PG conceptualized the research idea. XX and YL performed the methodology. YL was involved in formal analysis. YF, JY, and WX investigated the data and obtained the resources. YL and LP wrote the original draft. HL reviewed and edited the paper, supervised the project, and acquired the funds. HL and YL visualized the data. All authors have read and agreed to the published version of the manuscript.

FUNDING

This work was supported by the Guangdong Major Project of Basic and Applied Basic Research (No. 2020B0301030003).

ACKNOWLEDGMENTS

We would like to express our gratitude to those who contributed to the success of the GMGS4 expedition. We also appreciate the efforts of the editors and reviewers, who gave constructive comments and suggestions which greatly improved this manuscript and inspired in-depth discussion.

SUPPLEMENTARY MATERIAL

The Supplementary Material for this article can be found online at: https://www.frontiersin.org/articles/10.3389/feart.2022.836381/full#supplementary-material

REFERENCES

Aksu, A. E., Abrajano, T., Mudie, P. J., and Yaşar, D. (1999). Organic Geochemical and Palynological Evidence for Terrigenous Origin of the Organic Matter in Aegean Sea Sapropel S1. *Mar. Geology.* 153, 303–318. doi:10.1016/S0025-3227(98)00077-2

Alford, M. H., Peacock, T., MacKinnon, J. A., Nash, J. D., Buijsman, M. C., Centurioni, L. R., et al. (2015). The Formation and Fate of Internal Waves in the South China Sea. *Nature* 521 (7550), 65–69. doi:10.1038/nature14399

Allen, K. D., Wegener, G., Matthew Sublett, D., Jr, Bodnar, R. J., Feng, X., Wendt, J., et al. (2021). Biogenic Formation of Amorphous Carbon by Anaerobic Methanotrophs and Select Methanogens. *Sci. Adv.* 7, 1–13. doi:10.1126/sciadv.abg9739

Anderson, T. F., and Pratt, L. M. (1995). "Isotopic Evidence for the Origin of Organic Sulfur and Elemental Sulfur in marine Sediments," in *Geochemical Transformations of Sedimentary Sulfur*. Editors M. Vairavamurthy, M. A. A. Schoonen, T. I. Eglinton, G. W. Luther, and B. Manowitz (Washington D C: American Chemical Society Symposium Series). doi:10.1021/bk-1995-0612.ch021

Antler, G., Turchyn, A. V., Herut, B., and Sivan, O. (2015). A Unique Isotopic Fingerprint of Sulfate-Driven Anaerobic Oxidation of Methane. *Geology* 43 (7), 619–622. doi:10.1130/g36688.1

Arnaboldi, M., and Meyers, P. A. (2006). Patterns of Organic Carbon and Nitrogen Isotopic Compositions of Latest Pliocene Sapropels from Six Locations across the Mediterranean Sea. *Palaeogeogr. Palaeoclimatol. Palaeoecol.* 235 (1-3), 149–167. doi:10.1016/j.palaeo.2005.09.027

Berner, R. A. (1982). Burial of Organic Carbon and Pyrite Sulfur in the Modern Ocean: Its Geochemical and Environmental Significance. *Am. J. Sci.* 282, 451–473. doi:10.2475/ajs.282.4.451

Berner, R. A. (1984). Sedimentary Pyrite Formation: An Update. *Geochimica et Cosmochimica Acta* 48, 605–615. doi:10.1016/0016-7037(84)90089-9

Boetius, A., Ravenschlag, K., Schubert, C. J., Rickert, D., Widdel, F., Gieseke, A., et al. (2000). A marine Microbial Consortium Apparently Mediating Anaerobic Oxidation of Methane. *Nature* 407, 623–626. doi:10.1038/35036572

Borowski, W. S., Rodriguez, N. M., Paull, C. K., and Ussler, W. (2013). Are 34S-Enriched Authigenic Sulfide Minerals a Proxy for Elevated Methane Flux and Gas Hydrates in the Geologic Record? *Mar. Pet. Geology.* 43, 381–395. doi:10.1016/j.marpetgeo.2012.12.009

Brunner, B., and Bernasconi, S. M. (2005). A Revised Isotope Fractionation Model for Dissimilatory Sulfate Reduction in Sulfate Reducing Bacteria. *Geochimica et Cosmochimica Acta* 69 (20), 4759–4771. doi:10.1016/j.gca.2005.04.015

Calvert, S. E., and Fontugne, M. R. (1987). Stable Carbon Isotopic Evidence for the marine Origin of the Organic Matter in the Holocene Black Sea Sapropel. *Chem. Geology. Isotope Geosci. section* 66, 315–322. doi:10.1016/0168-9622(87)90051-0

Calvert, S. E., Nielsen, B., and Fontugne, M. R. (1992). Evidence from Nitrogen Isotope Ratios for Enhanced Productivity during Formation of Eastern Mediterranean Sapropels. *Nature* 359, 223–225. doi:10.1038/359223a0

Calvert, S. E. (2004). Beware Intercepts: Interpreting Compositional Ratios in Multi-Component Sediments and Sedimentary Rocks. *Org. Geochem.* 35 (8), 981–987. doi:10.1016/j.orggeochem.2004.03.001

Chen, C.-T. A., and Wang, S.-L. (1998). Influence of Intermediate Water in the Western Okinawa Trough by the Outflow from the South China Sea. *J. Geophys. Res.* 103 (C6), 12683–12688. doi:10.1029/98jc00366

Chen, H., Xie, X., Van Rooij, D., Vandorpe, T., Su, M., and Wang, D. (2014). Depositional Characteristics and Processes of Alongslope Currents Related to a Seamount on the Northwestern Margin of the Northwest Sub-Basin, South China Sea. *Mar. Geology.* 355, 36–53. doi:10.1016/j.margeo.2014.05.008

Collett, T. S., Johnson, A. H., Knapp, C. C., and Boswell, R. (2009). Natural Gas Hydrates: A Review. *AAPG Memoir* 89, 149–219. doi:10.1306/13201142M891602

Deusner, C., Holler, T., Arnold, G. L., Bernasconi, S. M., Formolo, M. J., and Brunner, B. (2014). Sulfur and Oxygen Isotope Fractionation during Sulfate Reduction Coupled to Anaerobic Oxidation of Methane Is Dependent on Methane Concentration. *Earth Planet. Sci. Lett.* 399, 61–73. doi:10.1016/j.epsl.2014.04.047

Emerson, S., and Hedges, J. I. (1988). Processes Controlling the Organic Carbon Content of Open Ocean Sediments. *Paleoceanography* 3 (5), 621–634. doi:10.1029/PA003i005p00621

Fang, G., Wang, G., Fang, Y., and Fang, W. (2012). A Review on the South China Sea Western Boundary Current. *Acta Oceanol. Sin.* 31 (5), 1–10. doi:10.1007/s13131-012-0231-y

Feng, D., Qiu, J.-W., Hu, Y., Peckmann, J., Guan, H., Tong, H., et al. (2018). Cold Seep Systems in the South China Sea: An Overview. *J. Asian Earth Sci.* 168, 3–16. doi:10.1016/j.jseaes.2018.09.021

Fontugne, M. R., and Duplessy, J.-C. (1986). Variations of the Monsoon Regime during the Upper Quaternary: Evidence from Carbon Isotopic Record of Organic Matter in north Indian Ocean Sediment Cores. *Palaeogeogr. Palaeoclimatol. Palaeoecol.* 56, 69–88. doi:10.1016/0031-0182(86)90108-2

Fontugne, M. R., and Jouanneau, J.-M. (1987). Modulation of the Particulate Organic Carbon Flux to the Ocean by a Macrotidal Estuary: Evidence from Measurements of Carbon Isotopes in Organic Matter from the Gironde System. *Estuarine, Coastal Shelf Sci.* 24 (3), 377–387. doi:10.1016/0272-7714(87)90057-6

Freudenthal, T., Wagner, T., Wenzhöfer, F., Zabel, M., and Wefer, G. (2001). Early Diagenesis of Organic Matter from Sediments of the Eastern Subtropical Atlantic: Evidence from Stable Nitrogen and Carbon Isotopes. *Geochimica et Cosmochimica Acta* 65, 1795–1808. doi:10.1016/S0016-7037(01)00554-3

Gaye, B., Wiesner, M. G., and Lahajnar, N. (2009). Nitrogen Sources in the South China Sea, as Discerned from Stable Nitrogen Isotopic Ratios in Rivers, Sinking Particles, and Sediments. *Mar. Chem.* 114 (3-4), 72–85. doi:10.1016/j.marchem.2009.04.003

Ge, Q., Chu, F., Xue, Z., Liu, J. P., Du, Y., and Fang, Y. (2010). Paleoenvironmental Records from the Northern South China Sea Since the Last Glacial Maximum. *Acta Oceanol. Sin.* 29 (3), 46–62. doi:10.1007/s13131-010-0036-9

Ge, Q., Liu, J. P., Xue, Z., and Chu, F. (2014). Dispersal of the Zhujiang River (Pearl River) Derived Sediment in the Holocene. *Acta Oceanol. Sin.* 33 (8), 1–9. doi:10.1007/s13131-014-0407-8

Geng, M. H., Song, H. B., Guan, Y. X., Bai, Y., Liu, S. X., and Chen, Y. W. (2017). The Distribution and Characteristics of Very Large Subaqueous Sand Dunes in the Dongsha Region of the Northern South China Sea. *Chin. J. Geophys-Ch* 60 (2), 628–638. (In Chinese with English Abstract). doi:10.6038/cjg20170217

Goñi, M. A., and Hedges, J. I. (1995). Sources and Reactivities of Marine-Derived Organic Matter in Coastal Sediments as Determined by Alkaline CuO Oxidation. *Geochimica et Cosmochimica Acta* 59, 2965–2981. doi:10.1016/0016-7037(95)00188-3

Greinert, J., Bohrmann, G., and Suess, E. (2001). "Gas Hydrate Associated Carbonates and Methane-Venting at Hydrate Ridge: Classification, Distribution and Origin of Authigenic Lithologies," in *Natural Gas*

Hydrates: Occurrence, Distribution, and Detection. Editors C. K. Paull and W. P. Dillon (Washington, DC, USA: American Geophysical Union).

He, D., Hou, D., Zhang, P., Harris, M., Mi, J., Chen, T., et al. (2016). Reservoir Characteristics in the LW3-1 Structure in the deepwater Area of the Baiyun Sag, South China Sea. *Arab J. Geosci.* 9 (4), 251. doi:10.1007/s12517-015-2279-4

Hedges, J. I., and Mann, D. C. (1979). The Lignin Geochemistry of marine Sediments from the Southern Washington Coast. *Geochimica et Cosmochimica Acta* 43, 1809–1818. doi:10.1016/0016-7037(79)90029-2

Higginson, M. J., Maxwell, J. R., and Altabet, M. A. (2003). Nitrogen Isotope and Chlorin Paleoproductivity Records from the Northern South China Sea: Remote vs. Local Forcing of Millennial- and Orbital-Scale Variability. *Mar. Geol.* 201 (1-3), 223–250. doi:10.1016/s0025-3227(03)00218-4

Hill, T. M., Kennett, J. P., and Valentine, D. L. (2004). Isotopic Evidence for the Incorporation of Methane-Derived Carbon into Foraminifera from Modern Methane Seeps, Hydrate Ridge, Northeast Pacific. *Geochimica et Cosmochimica Acta* 68 (22), 4619–4627. doi:10.1016/j.gca.2004.07.012

Hill, T. M., Paull, C. K., and Critser, R. B. (2011). Glacial and Deglacial Seafloor Methane Emissions from Pockmarks on the Northern Flank of the Storegga Slide Complex. *Geo-Mar. Lett.* 32 (1), 73–84. doi:10.1007/s00367-011-0258-7

Hsü, M. K., Liu, A. K., and Liu, C. (2000). A Study of Internal Waves in the China Seas and Yellow Sea Using SAR. *Cont. Shelf Res.* 20, 389–410. doi:10.1016/S0278-4343(99)00078-3

Hu, J., Peng, P. a., Jia, G., Mai, B., and Zhang, G. (2006). Distribution and Sources of Organic Carbon, Nitrogen and Their Isotopes in Sediments of the Subtropical Pearl River Estuary and Adjacent Shelf, Southern China. *Mar. Chem.* 98 (2-4), 274–285. doi:10.1016/j.marchem.2005.03.008

Hu, Y., Feng, D., Peng, Y., Peckmann, J., Kasten, S., Wang, X., et al. (2020). A Prominent Isotopic Fingerprint of Nitrogen Uptake by Anaerobic Methanotrophic Archaea. *Chem. Geology.* 558, 119972. doi:10.1016/j.chemgeo.2020.119972

Hu, Z., Huang, B.-Q., Liu, L.-J., and Wang, N. (2021). Spatiotemporal Patterns of Sediment Deposition on the Northern Slope of the South China Sea in the Last 150,000 Years. *J. Palaeogeogr.* 10 (1), 21. doi:10.1186/s42501-021-00102-3

Huang, J., Li, A., and Wan, S. (2011). Sensitive Grain-Size Records of Holocene East Asian Summer Monsoon in Sediments of Northern South China Sea Slope. *Quat. Res.* 75 (3), 734–744. doi:10.1016/j.yqres.2011.03.002

Huang, J., Wan, S., Xiong, Z., Zhao, D., Liu, X., Li, A., et al. (2016). Geochemical Records of Taiwan-Sourced Sediments in the South China Sea Linked to Holocene Climate Changes. *Palaeogeogr. Palaeoclimatol. Palaeoecol.* 441, 871–881. doi:10.1016/j.palaeo.2015.10.036

Huh, C.-A., Liu, J. T., Lin, H.-L., and Xu, J. P. (2009). Tidal and Flood Signatures of Settling Particles in the Gaoping Submarine Canyon (SW Taiwan) Revealed from Radionuclide and Flow Measurements. *Mar. Geology.* 267 (1-2), 8–17. doi:10.1016/j.margeo.2009.09.001

Jasper, J. P., and Gagosian, R. B. (1989). Glacial-Interglacial Climatically Forced δ13C Variations in Sedimentary Organic Matter. *Nature* 342, 60–62. doi:10.1038/342060a0

Jiang, H., Pang, X., Shi, H., Yu, Q., Cao, Z., Yu, R., et al. (2015). Source Rock Characteristics and Hydrocarbon Expulsion Potential of the Middle Eocene Wenchang Formation in the Huizhou Depression, Pearl River Mouth basin, south China Sea. *Mar. Pet. Geology.* 67, 635–652. doi:10.1016/j.marpetgeo.2015.06.010

Jørgensen, B. B., Böttcher, M. E., Lüschen, H., Neretin, L. N., and Volkov, I. I. (2004). Anaerobic Methane Oxidation and a Deep H2S Sink Generate Isotopically Heavy Sulfides in Black Sea Sediments. *Geochimica et Cosmochimica Acta* 68 (9), 2095–2118. doi:10.1016/j.gca.2003.07.017

Jørgensen, B. B., Findlay, A. J., and Pellerin, A. (2019). The Biogeochemical Sulfur Cycle of Marine Sediments. *Front. Microbiol.* 10, 849. doi:10.3389/fmicb.2019.00849

Jørgensen, B. B. (1982). Mineralization of Organic Matter in the Sea Bed-The Role of Sulphate Reduction. *Nature* 296, 643–645. doi:10.1038/296643a0

Jørgensen, B. B. (2021). Sulfur Biogeochemical Cycle of Marine Sediments. *Geochem. Persp.* 10, 145–307. doi:10.7185/geochempersp.10.2

Joseph, C., Campbell, K. A., Torres, M. E., Martin, R. A., Pohlman, J. W., Riedel, M., et al. (2013). Methane-Derived Authigenic Carbonates from Modern and Paleoseeps on the Cascadia Margin: Mechanisms of Formation and Diagenetic Signals. *Palaeogeogr. Palaeoclimatol. Palaeoecol.* 390, 52–67. doi:10.1016/j.palaeo.2013.01.012

Kaneko, M., Shingai, H., Pohlman, J. W., and Naraoka, H. (2010). Chemical and Isotopic Signature of Bulk Organic Matter and Hydrocarbon Biomarkers within Mid-Slope Accretionary Sediments of the Northern Cascadia Margin Gas Hydrate System. *Mar. Geology.* 275 (1-4), 166–177. doi:10.1016/j.margeo.2010.05.010

Kao, S.-J., Shiah, F.-K., Wang, C.-H., and Liu, K.-K. (2006). Efficient Trapping of Organic Carbon in Sediments on the continental Margin with High Fluvial Sediment Input off Southwestern Taiwan. *Continental Shelf Res.* 26 (20), 2520–2537. doi:10.1016/j.csr.2006.07.030

Kao, S.-J., Terence Yang, J.-Y., Liu, K.-K., Dai, M., Chou, W.-C., Lin, H.-L., et al. (2012). Isotope Constraints on Particulate Nitrogen Source and Dynamics in the Upper Water Column of the Oligotrophic South China Sea. *Glob. Biogeochem. Cycles* 26 (2), GB2033. doi:10.1029/2011gb004091

Kienast, M., Higginson, M. J., Mollenhauer, G., Eglinton, T. I., Chen, M.-T., and Calvert, S. E. (2005). On the Sedimentological Origin of Down-Core Variations of Bulk Sedimentary Nitrogen Isotope Ratios. *Paleoceanography* 20 (2), 1–13. doi:10.1029/2004pa001081

Kienast, M. (2000). Unchanged Nitrogen Isotopic Composition of Organic Matter in the South China Sea during the Last Climatic Cycle: Global Implications. *Paleoceanography* 15 (2), 244–253. doi:10.1029/1999pa000407

Kvenvolden, K. A. (1995). A Review of the Geochemistry of Methane in Natural Gas Hydrate. *Org. Geochem.* 23, 997–1008. doi:10.1016/0146-6380(96)00002-2

Lehmann, M. F., Bernasconi, S. M., Barbieri, A., and Mckenzie, J. A. (2002). Preservation of Organic Matter and Alteration of its Carbon and Nitrogen Isotope Composition during Simulated and *In Situ* Early Sedimentary Diagenesis. *Geochimica et Cosmochimica Acta* 66, 3573–3584. doi:10.1016/S0016-7037(02)00968-7

Lehmann, M. F., Sigman, D. M., McCorkle, D. C., Granger, J., Hoffmann, S., Cane, G., et al. (2007). The Distribution of Nitrate 15N/14N in marine Sediments and the Impact of Benthic Nitrogen Loss on the Isotopic Composition of Oceanic Nitrate. *Geochimica et Cosmochimica Acta* 71 (22), 5384–5404. doi:10.1016/j.gca.2007.07.025

Li, Q. Y., Zhao, Q. H., Zhong, G. F., Jian, Z. M., Tian, J., Cheng, X. R., et al. (2007). Deepwater Ventilation and Stratification in the Neogene South China Sea. *J. China Univ. Geosci.* 18 (2), 95–108. doi:10.1016/s1002-0705(07)60024-7

Lin, F., Hou, Y., Liu, Y., Fang, Y., and Hu, P. (2014). Internal Solitary Waves on the Southwest Shelf of Dongsha Island Observed from Mooring ADCP. *Chin. J. Ocean. Limnol.* 32 (5), 1179–1187. doi:10.1007/s00343-014-3254-8

Lin, Z., Sun, X., Peckmann, J., Lu, Y., Xu, L., Strauss, H., et al. (2016). How Sulfate-Driven Anaerobic Oxidation of Methane Affects the Sulfur Isotopic Composition of Pyrite: A SIMS Study from the South China Sea. *Chem. Geology.* 440, 26–41. doi:10.1016/j.chemgeo.2016.07.007

Liu, K.-K., Kao, S.-J., Hu, H.-C., Chou, W.-C., Hung, G.-W., and Tseng, C.-M. (2007a). Carbon Isotopic Composition of Suspended and Sinking Particulate Organic Matter in the Northern South China Sea-From Production to Deposition. *Deep Sea Res. Part. Topical Studi. Oceanography* 54 (14-15), 1504–1527. doi:10.1016/j.dsr2.2007.05.010

Liu, Z., Colin, C., Huang, W., Le, K. P., Tong, S., Chen, Z., et al. (2007b). Climatic and Tectonic Controls on Weathering in south China and Indochina Peninsula: Clay Mineralogical and Geochemical Investigations from the Pearl, Red, and Mekong Drainage Basins. *Geochem. Geophys. Geosyst.* 8 (5), 1–18. doi:10.1029/2006gc001490

Liu, Z., Colin, C., Huang, W., Chen, Z., Trentesaux, A., and Chen, J. (2008). Clay Minerals in Surface Sediments of the Pearl River Drainage basin and Their Contribution to the South China Sea. *Chin. Sci. Bull.* 52 (8), 1101–1111. doi:10.1007/s11434-007-0161-9

Liu, Z., Zhao, Y., Colin, C., Siringan, F. P., and Wu, Q. (2009). Chemical Weathering in Luzon, Philippines from clay Mineralogy and Major-Element Geochemistry of River Sediments. *Appl. Geochem.* 24 (11), 2195–2205. doi:10.1016/j.apgeochem.2009.09.025

Liu, J., Chen, M., Chen, Z., and Yan, W. (2010a). Clay Mineral Distribution in Surface Sediments of the South China Sea and its Significance for in Sediment Sources and Transport. *Chin. J. Ocean. Limnol.* 28 (2), 407–415. doi:10.1007/s00343-010-9057-7

Liu, Z., Colin, C., Li, X., Zhao, Y., Tuo, S., Chen, Z., et al. (2010b). Clay mineral Distribution in Surface Sediments of the Northeastern South China Sea and Surrounding Fluvial Drainage Basins: Source and Transport. *Mar. Geology.* 277 (1-4), 48–60. doi:10.1016/j.margeo.2010.08.010

Liu, H., Yao, Y., and Deng, H. (2011a). Geological and Geophysical Conditions for Potential Natural Gas Hydrate Resources in Southern South China Sea Waters. *J. Earth Sci.* 22 (6), 718–725. doi:10.1007/s12583-011-0222-5

Liu, J., Xiang, R., Chen, M., Chen, Z., Yan, W., and Liu, F. (2011b). Influence of the Kuroshio Current Intrusion on Depositional Environment in the Northern South China Sea: Evidence from Surface Sediment Records. *Mar. Geology.* 285 (1-4), 59–68. doi:10.1016/j.margeo.2011.05.010

Liu, J., Xiang, R., Chen, Z., Chen, M., Yan, W., Zhang, L., et al. (2013). Sources, Transport and Deposition of Surface Sediments from the South China Sea. *Deep Sea Res. Part Oceanographic Res. Pap.* 71, 92–102. doi:10.1016/j.dsr.2012.09.006

Liu, J., Clift, P. D., Yan, W., Chen, Z., Chen, H., Xiang, R., et al. (2014). Modern Transport and Deposition of Settling Particles in the Northern South China Sea: Sediment Trap Evidence Adjacent to Xisha Trough. *Deep Sea Res. Oceanographic Res. Pap.* 93, 145–155. doi:10.1016/j.dsr.2014.08.005

Liu, Z., Zhao, Y., Colin, C., Stattegger, K., Wiesner, M. G., Huh, C.-A., et al. (2016). Source-to-Sink Transport Processes of Fluvial Sediments in the South China Sea. *Earth-Science Rev.* 153, 238–273. doi:10.1016/j.earscirev.2015.08.005

Liu, J., Steinke, S., Vogt, C., Mohtadi, M., De Pol-Holz, R., and Hebbeln, D. (2017). Temporal and Spatial Patterns of Sediment Deposition in the Northern South China Sea over the Last 50,000 Years. *Palaeogeogr. Palaeoclimatol. Palaeoecol.* 465, 212–224. doi:10.1016/j.palaeo.2016.10.033

Liu, X., Fike, D., Li, A., Dong, J., Xu, F., Zhuang, G., et al. (2019). Pyrite Sulfur Isotopes Constrained by Sedimentation Rates: Evidence from Sediments on the East China Sea Inner Shelf since the Late Pleistocene. *Chem. Geology.* 505, 66–75. doi:10.1016/j.chemgeo.2018.12.014

Liu, J., Pellerin, A., Antler, G., Kasten, S., Findlay, A. J., Dohrmann, I., et al. (2020). Early Diagenesis of Iron and Sulfur in Bornholm Basin Sediments: The Role of Near-Surface Pyrite Formation. *Geochimica et Cosmochimica Acta* 284, 43–60. doi:10.1016/j.gca.2020.06.003

Liu, X., Zhang, M., Li, A., Fan, D., Dong, J., Jiao, C., et al. (2021). Depositional Control on Carbon and Sulfur Preservation Onshore and Offshore the Oujiang Estuary: Implications for the C/S Ratio as a Salinity Indicator. *Continental Shelf Res.* 227, 104510. doi:10.1016/j.csr.2021.104510

Lüdmann, T. (2005). Upward Flow of North Pacific Deep Water in the Northern South China Sea as Deduced from the Occurrence of Drift Sediments. *Geophys. Res. Lett.* 32, 1–4. doi:10.1029/2004gl021967

Lu, H. F., Chen, H., Chen, F., and Liao, Z. L. (2009). Mineralogy of the Sediments from Gas-Hydrate Drilling Sites, Shenhu Area, South China Sea. *Geol. Study South China Sea*, 28–39. (In Chinese with English Abstract).

Lu, H. F., Sun, X. M., and Zhang, M. (2011). *Mineralogy and Geochemistry of NGH Deposits in the south China Sea*. Beijing: Science Press.

Lu, Y., Sun, X., Xu, H., Konishi, H., Lin, Z., Xu, L., et al. (2018). Formation of Dolomite Catalyzed by Sulfate-Driven Anaerobic Oxidation of Methane: Mineralogical and Geochemical Evidence from the Northern South China Sea. *Am. Mineral.* 103 (5), 720–734. doi:10.2138/am-2018-6226

Ma, X., Yan, J., Hou, Y., Lin, F., and Zheng, X. (2016). Footprints of Obliquely Incident Internal Solitary Waves and Internal Tides Near the Shelf Break in the Northern South China Sea. *J. Geophys. Res. Oceans* 121 (12), 8706–8719. doi:10.1002/2016jc012009

McArthur, J. M., Tyson, R. V., Thomson, J., and Mattey, D. (1992). Early Diagenesis of marine Organic Matter: Alteration of the Carbon Isotopic Composition. *Mar. Geology.* 105, 51–61. doi:10.1016/0025-3227(92)90181-G

Meyers, P. A. (1994). Preservation of Elemental and Isotopic Source Identification of Sedimentary Organic Matter. *Chem. Geology.* 114, 289–302. doi:10.1016/0009-2541(94)90059-0

Meyers, P. A. (1997). Organic Geochemical Proxies of Paleoceanographic, Paleolimnologic, and Paleoclimatic Processes. *Org. Geochem.* 27, 213–250. doi:10.1016/S0146-6380(97)00049-1

Milliman, J. D., and Farnsworth, K. L. (2011). *River Discharge to the Coastal Ocean: A Global Synthesis*. Cambridge: Cambridge University Press.

Milliman, J. D., and Meade, R. H. (1983). World-Wide Delivery of River Sediment to the Oceans. *J. Geology.* 91, 1–21. doi:10.1086/628741

Müller, P. J. (1977). C/N Ratios in Pacific Deep-Sea Sediments: Effect of Inorganic Ammonium and Organic Nitrogen Compounds Sorbed by Clays. *Geochim. Cosmochim. Acta* 41, 765–776. doi:10.1016/0016-7037(77)90047-3

Nan, F., Xue, H., and Yu, F. (2015). Kuroshio Intrusion into the South China Sea: A Review. *Prog. Oceanography* 137, 314–333. doi:10.1016/j.pocean.2014.05.012

Nijenhuis, I. A., and De Lange, G. J. (2000). Geochemical Constraints on Pliocene Sapropel Formation in the Eastern Mediterranean. *Mar. Geology.* 163, 41–63. doi:10.1016/S0025-3227(99)00093-6

O'Leary, M. H. (1988). Carbon Isotopes in Photosynthesis. *BioScience* 38 (5), 328–336. doi:10.2307/1310735

Pang, X., Chen, C., Peng, D., Zhu, M., Shu, Y., He, M., et al. (2007). Sequence Stratigraphy of Deep-Water Fan System of Pearl River, South China Sea. *Earth Sci. Front.* 14 (1), 220–229. doi:10.1016/s1872-5791(07)60010-4

Peckmann, J., and Thiel, V. (2004). Carbon Cycling at Ancient Methane-Seeps. *Chem. Geology.* 205 (3-4), 443–467. doi:10.1016/j.chemgeo.2003.12.025

Peckmann, J., Reimer, A., Luth, U., Luth, C., Hansen, B. T., Heinicke, C., et al. (2001). Methane-Derived Carbonates and Authigenic Pyrite from the Northwestern Black Sea. *Mar. Geology.* 177, 129–150. doi:10.1016/S0025-3227(01)00128-1

Peketi, A., Mazumdar, A., Joshi, R. K., Patil, D. J., Srinivas, P. L., and Dayal, A. M. (2012). Tracing the Paleo Sulfate-Methane Transition Zones and H2S Seepage Events in marine Sediments: An Application of C-S-Mo Systematics. *Geochem. Geophys. Geosyst.* 13, Q10007. doi:10.1029/2012gc004288

Peketi, A., Mazumdar, A., Joao, H. M., Patil, D. J., Usapkar, A., and Dewangan, P. (2015). Coupled C-S-Fe Geochemistry in a Rapidly Accumulating marine Sedimentary System: Diagenetic and Depositional Implications. *Geochem. Geophys. Geosyst.* 16 (9), 2865–2883. doi:10.1002/2015gc005754

Prahl, F. G., Ertel, J. R., Goni, M. A., Sparrow, M. A., and Eversmeyer, B. (1994). Terrestrial Organic Carbon Contributions to Sediments on the Washington Margin. *Geochimica et Cosmochimica Acta* 58 (14), 3035–3048. doi:10.1016/0016-7037(94)90177-5

Premuzic, E. T., Benkovitz, C. M., Gaffney, J. S., and Walsh, J. J. (1982). The Nature and Distribution of Organic Matter in the Surface Sediments of World Oceans and Seas. *Org. Geochem.* 4, 62–77. doi:10.1016/0146-6380(82)90009-2

Qu, T., Girton, J. B., and Whitehead, J. A. (2006). Deepwater Overflow through Luzon Strait. *J. Geophys. Res.* 111, C01002. doi:10.1029/2005jc003139

Reeder, D. B., Ma, B. B., and Yang, Y. J. (2011). Very Large Subaqueous Sand Dunes on the Upper continental Slope in the South China Sea Generated by Episodic, Shoaling Deep-Water Internal Solitary Waves. *Mar. Geology.* 279 (1-4), 12–18. doi:10.1016/j.margeo.2010.10.009

Rodriguez, N. M., Paull, C. K., and Borowski, W. S. (2000). *Zonation of Authigenic Carbonates within Gas-Hydrate-Bearing Sedimentary Sections on the Blake Ridge*. College Station, TX: offshore southeastern North America.

Sackett, W. M., and Thompson, R. R. (1963). Isotopic Organic Carbon Composition of Recent continental Derived Clastic Sediments of Eastern Gulf Coast, Gulf of Mexico. *AAPG Bull.* 47, 525–531. doi:10.1306/bc743a5f-16be-11d7-8645000102c1865d

Saito, H., and Suzuki, N. (2007). Terrestrial Organic Matter Controlling Gas Hydrate Formation in the Nankai Trough Accretionary Prism, Offshore Shikoku, Japan. *J. Geochemical Exploration* 95 (1-3), 88–100. doi:10.1016/j.gexplo.2007.05.007

Schoell, M. (1983). Genetic Characterization of Natural Gases. *Bulletin* 67, 229–230. doi:10.1306/AD46094A-16F7-11D7-8645000102C1865D

Schroeder, A., Wiesner, M. G., and Liu, Z. (2015). Fluxes of clay Minerals in the South China Sea. *Earth Planet. Sci. Lett.* 430, 30–42. doi:10.1016/j.epsl.2015.08.001

Schubert, C. J., and Calvert, S. E. (2001). Nitrogen and Carbon Isotopic Composition of marine and Terrestrial Organic Matter in Arctic Ocean Sediments:. *Deep Sea Res. Part Oceanographic Res. Pap.* 48, 789–810. doi:10.1016/S0967-0637(00)00069-8

Shao, L., Li, X., Wei, G., Liu, Y., and Fang, D. (2001). Provenance of a Prominent Sediment Drift on the Northern Slope of the South China Sea. *Sci. China Ser. D-earth Sci.* 44, 919–925. doi:10.1007/BF02907084

Shawar, L., Halevy, I., Said-Ahmad, W., Feinstein, S., Boyko, V., Kamyshny, A., et al. (2018). Dynamics of Pyrite Formation and Organic Matter Sulfurization in Organic-Rich Carbonate Sediments. *Geochimica et Cosmochimica Acta* 241, 219–239. doi:10.1016/j.gca.2018.08.048

Sim, M. S., Bosak, T., and Ono, S. (2011). Large Sulfur Isotope Fractionation Does Not Require Disproportionation. *Science* 333, 74–77. doi:10.1126/science.1205103

Su, P., Liang, J., Peng, J., Zhang, W., and Xu, J. (2018). Petroleum Systems Modeling on Gas Hydrate of the First Experimental Exploitation Region in the Shenhu Area, Northern South China Sea. *J. Asian Earth Sci.* 168, 57–76. doi:10.1016/j.jseaes.2018.08.001

Su, M., Alves, T. M., Li, W., Sha, Z., Hsiung, K.-H., Liang, J., et al. (2019). Reassessing Two Contrasting Late Miocene-Holocene Stratigraphic Frameworks for the Pearl River Mouth Basin, Northern South China Sea. *Mar. Pet. Geology.* 102, 899–913. doi:10.1016/j.marpetgeo.2018.12.034

Su, M., Lin, Z., Wang, C., Kuang, Z., Liang, J., Chen, H., et al. (2020). Geomorphologic and Infilling Characteristics of the Slope-Confined Submarine Canyons in the Pearl River Mouth Basin, Northern South China Sea. *Mar. Geology.* 424, 106166. doi:10.1016/j.margeo.2020.106166

Su, M., Luo, K., Fang, Y., Kuang, Z., Yang, C., Liang, J., et al. (2021). Grain-Size Characteristics of fine-grained Sediments and Association with Gas Hydrate Saturation in Shenhu Area, Northern South China Sea. *Ore Geology. Rev.* 129, 103889. doi:10.1016/j.oregeorev.2020.103889

Sun, Z., Zhou, D., Zhong, Z., Xia, B., Qiu, X., Zeng, Z., et al. (2006). Research on the Dynamics of the South China Sea Opening: Evidence from Analogue Modeling. *Sci. China Ser. D* 49 (10), 1053–1069. doi:10.1007/s11430-006-1053-6

Tang, Q., Xu, M., Zheng, C., Xu, X., and Xu, J. (2018). A Locally Generated High-Mode Nonlinear Internal Wave Detected on the Shelf of the Northern South China Sea from Marine Seismic Observations. *J. Geophys. Res. Oceans* 123 (2), 1142–1155. doi:10.1002/2017jc013347

Tian, J., Yang, Q., Liang, X., Xie, L., Hu, D., Wang, F., et al. (2006). Observation of Luzon Strait Transport. *Geophys. Res. Lett.* 33 (19), L19607. doi:10.1029/2006gl026272

Trung, N. N. (2012). The Gas Hydrate Potential in the South China Sea. *J. Pet. Sci. Eng.* 88-89, 41–47. doi:10.1016/j.petrol.2012.01.007

Ussler, W., and Paull, C. K. (2008). Rates of Anaerobic Oxidation of Methane and Authigenic Carbonate Mineralization in Methane-Rich Deep-Sea Sediments Inferred from Models and Geochemical Profiles. *Earth Planet. Sci. Lett.* 266 (3-4), 271–287. doi:10.1016/j.epsl.2007.10.056

Wan, S., Li, A., Clift, P. D., Wu, S., Xu, K., and Li, T. (2010). Increased Contribution of Terrigenous Supply from Taiwan to the Northern South China Sea since 3Ma. *Mar. Geology.* 278 (1-4), 115–121. doi:10.1016/j.margeo.2010.09.008

Wang, D., Hong, B., Gan, J., and Xu, H. (2010). Numerical Investigation on Propulsion of the Counter-wind Current in the Northern South China Sea in winter. *Deep Sea Res. Part Oceanographic Res. Pap.* 57 (10), 1206–1221. doi:10.1016/j.dsr.2010.06.007

Wang, J., Huang, W., Yang, J., Zhang, H., and Zheng, G. (2012). Study of the Propagation Direction of the Internal Waves in the South China Sea Using Satellite Images. *Acta Oceanol. Sin.* 32 (5), 42–50. doi:10.1007/s13131-013-0312-6

Wang, X., Collett, T. S., Lee, M. W., Yang, S., Guo, Y., and Wu, S. (2014). Geological Controls on the Occurrence of Gas Hydrate from Core, Downhole Log, and Seismic Data in the Shenhu Area, South China Sea. *Mar. Geology.* 357, 272–292. doi:10.1016/j.margeo.2014.09.040

Wang, T., Ravelo, A. C., Ren, H., Dang, H., Jin, H., Liu, J., et al. (2018). Nitrogen Isotope Variations in the Northern South China Sea Since Marine Isotopic Stage 3: Reconstructed from Foraminifera-Bound and Bulk Sedimentary Nitrogen. *Paleoceanogr. Paleoclimatol.* 33 (6), 594–605. doi:10.1029/2018pa003344

Wang, P., Li, S., Suo, Y., Guo, L., Wang, G., Hui, G., et al. (2020a). Plate Tectonic Control on the Formation and Tectonic Migration of Cenozoic Basins in Northern Margin of the South China Sea. *Geosci. Front.* 11 (4), 1231–1251. doi:10.1016/j.gsf.2019.10.009

Wang, X., Kneller, B., Wang, Y., and Chen, W. (2020b). Along-Strike Quaternary Morphological Variation of the Baiyun Sag, South China Sea: The Interplay between Deltas, Pre-existing Morphology, and Oceanographic Processes. *Mar. Pet. Geology.* 122, 104640. doi:10.1016/j.marpetgeo.2020.104640

Wang, P. (2003). Evolution of the South China Sea and Monsoon History Revealed in Deep-Sea Records. *Chin. Sci Bull* 48 (23), 2549. doi:10.1360/03wd0156

Wing, B. A., and Halevy, I. (2014). Intracellular Metabolite Levels Shape Sulfur Isotope Fractionation during Microbial Sulfate Respiration. *Proc. Natl. Acad. Sci. USA* 111 (51), 18116–18125. doi:10.1073/pnas.1407502111

Wong, G. T. F., Chung, S.-W., Shiah, F.-K., Chen, C.-C., Wen, L.-S., and Liu, K.-K. (2002). Nitrate Anomaly in the Upper Nutricline in the Northern South China Sea - Evidence for Nitrogen Fixation. *Geophys. Res. Lett.* 29 (23), 12–11214. doi:10.1029/2002gl015796

Wu, N., Zhang, H., Yang, S., Zhang, G., Liang, J., Lu, J. a., et al. (2011). Gas Hydrate System of Shenhu Area, Northern South China Sea: Geochemical Results. *J. Geol. Res.* 2011, 1–10. doi:10.1155/2011/370298

Xiao, Q. W., Feng, X. L., and Miao, X. M. (2021). Turbidity Deposits and Their Provenance: Evidence from Core SH37 in Shenhu Area of the South China Sea. *Mar. Geol. Quat. Geol.* 41, 101–111. (in Chinese with English Abstract). doi:10.16562/j.cnki.0256-1492.2021011901

Xu, J., Ben-Avraham, Z., Kelty, T., and Yu, H.-S. (2014a). Origin of Marginal Basins of the NW Pacific and Their Plate Tectonic Reconstructions. *Earth-Science Rev.* 130, 154–196. doi:10.1016/j.earscirev.2013.10.002

Xu, W., Yan, W., Chen, Z., Chen, H., Huang, W., and Lin, T. (2014b). Organic Matters and Lipid Biomarkers in Surface Sediments from the Northern South China Sea: Origins and Transport. *J. Earth Sci.* 25 (1), 189–196. doi:10.1007/s12583-014-0412-z

Yang, J.-Y. T., Kao, S.-J., Dai, M., Yan, X., and Lin, H.-L. (2017a). Examining N Cycling in the Northern South China Sea from N Isotopic Signals in Nitrate and Particulate Phases. *J. Geophys. Res. Biogeosci.* 122 (8), 2118–2136. doi:10.1002/2016jg003618

Yang, S. X., Lei, Y., Liang, J. Q., Holland, M., Schultheiss, P., Lu, J. A., et al. (2017b). "Concentrated Gas Hydrate in the Shenhu Area, South China Sea: Results from Drilling Expeditions GMGS3 & GMGS4," in Proceedings of 9th International Conference on Gas Hydrates (ICGH 2017), Denver, CO, June 25–30, 2017.

Yu, X., Li, J., Gong, J., Chen, J., Jin, X., Lee, Y.-J., et al. (2006). Stable Carbon and Nitrogen Isotopic Composition of Gas Hydrate-Bearing Sediment from Hydrate Ridge, Cascadia Margin. *Sci. China Ser. D* 49 (8), 872–880. doi:10.1007/s11430-006-0872-9

Yu, H. S. (1990). The Pearl River Mouth basin: A Rift basin and its Geodynamic Relationship with the southeastern Eurasian Margin. *Tectonophysics* 183, 177–186. doi:10.1016/0040-1951(90)90415-5

Zhang, G. C., Yang, H. C., Chen, Y., Ji, M., Wang, K., Yang, D. S., et al. (2014a). The Baiyun Sag: A Giant Rich Gas-Generation Sag in the Deepwater Area of the Pearl River Mouth Basin. *Nat. Gas. Ind.* 34, 11–25. (in Chinese with English abstract). doi:10.3787/j.issn.1000-0976.2014.11.002

Zhang, Y., Kaiser, K., Li, L., Zhang, D., Ran, Y., and Benner, R. (2014b). Sources, Distributions, and Early Diagenesis of Sedimentary Organic Matter in the Pearl River Region of the South China Sea. *Mar. Chem.* 158, 39–48. doi:10.1016/j.marchem.2013.11.003

Zhang, Y., Liu, Z., Zhao, Y., Wang, W., Li, J., and Xu, J. (2014c). Mesoscale Eddies Transport Deep-Sea Sediments. *Sci. Rep.* 4, 5937. doi:10.1038/srep05937

Zhang, W., Liang, J., Lu, J. A., Wei, J., Su, P., Fang, Y., et al. (2017a). Accumulation Features and Mechanisms of High Saturation Natural Gas Hydrate in Shenhu Area, Northern South China Sea. *Pet. Exploration Develop.* 44 (5), 708–719. doi:10.1016/s1876-3804(17)30082-4

Zhang, X., He, J., Zhao, Y., Wu, H., and Ren, Z. (2017b). Geochemical Characteristics and Origins of the Crude Oil of Triassic Yanchang Formation in Southwestern Yishan Slope, Ordos Basin. *Int. J. Anal. Chem.* 2017, 1–12. doi:10.1155/2017/6953864

Zhang, W., Liang, J., Wei, J., Su, P., Lin, L., and Huang, W. (2019). Origin of Natural Gases and Associated Gas Hydrates in the Shenhu Area, Northern South China Sea: Results from the China Gas Hydrate Drilling Expeditions. *J. Asian Earth Sci.* 183, 103953. doi:10.1016/j.jseaes.2019.103953

Zhao, Z., and Alford, M. H. (2006). Source and Propagation of Internal Solitary Waves in the Northeastern South China Sea. *J. Geophys. Res.* 111, C11012. doi:10.1029/2006jc003644

Zhu, M., Graham, S., Pang, X., and McHargue, T. (2010). Characteristics of Migrating Submarine Canyons from the Middle Miocene to Present: Implications for Paleoceanographic Circulation, Northern South China Sea. *Mar. Pet. Geology.* 27 (1), 307–319. doi:10.1016/j.marpetgeo.2009.05.005

Conflict of Interest: The authors declare that the research was conducted in the absence of any commercial or financial relationships that could be construed as a potential conflict of interest.

Publisher's Note: All claims expressed in this article are solely those of the authors and do not necessarily represent those of their affiliated organizations, or those of the publisher, the editors, and the reviewers. Any product that may be evaluated in this article, or claim that may be made by its manufacturer, is not guaranteed or endorsed by the publisher.